LRP 515/95 April 1995

RELATIVE CALIBRATION OF PHOTODIODES IN THE SOFT-X-RAY SPECTRAL RANGE

M. Anton, M.J. Dutch, H. Weisen

submitted for publication to
Rev. Sci. Instrum.

Relative Calibration of Photodiodes in the Soft-X-ray Spectral Range

M. Anton, M. J. Dutch and H. Weisen

Centre de Recherches en Physique des Plasmas
École Polytechnique Fédérale de Lausanne
Association EURATOM — Confédération Suisse
Avenue des Bains 21, CH-1007 Lausanne, Switzerland

Abstract

A method of obtaining a relative calibration of Si-photodiodes for the spectral range of soft X-rays ($1 - 30keV$) is presented. A simple mathematical model of the pn-diode is adopted which allows the response to be described in terms of a small set of parameters. The diffusion length as well as the thickness of a dead layer below the front surface of the diodes are obtained from measurements of angular dependences of the photoinduced current. We show that a precise characterisation of the diode response and an accurate relative calibration can be obtained using this method. However, we find that the presence of a dead layer a few tenths of a μm thick can pose severe restrictions on the use of planar diode arrays in X-ray tomography systems where uniformity of response is crucial. The method has been applied to the diode arrays equipping the X-ray tomography system built for the TCV tokamak, a magnetic fusion research device.

1 Introduction

Soft-X-ray tomography is an important diagnostic for magnetically confined hot plasmas. Tomographic inversion of line integrated measurements of X-ray emission in the spectral range between $1keV$ and $10keV$ reveals the 2D topology of the emissivity distribution in a poloidal cross section. It allows the study of MHD-activity and plasma shape with a fast time response as well as estimations of impurity levels or of radiation losses in the plasma core.

The instrumentation generally consists of a set of pinhole cameras with a set of chordal views in a fan-like geometry. The first cameras built and used for X-ray tomography on tokamak devices contained single PIN-diodes or surface barrier detectors. The advantage of single detectors is that they can always be oriented such that their surface is normal to the incident radiation. A drawback is the limited number of available channels because of the usually very restricted space in a tokamak or stellarator environment. To overcome this disadvantage, the use of very compact, commercially available arrays of 16-38 photodiodes has become popular since they were first used successfully by *Camacho and Granetz* in 1986 [1]. The arrays allow the use of 100-200 detector channels with minimal space requirements. A schematic drawing of a pinhole camera with a planar detector array is shown in figure 1.

The experimental data is usually a set of line-integrated measure-

ments, the so-called chord brightnesses f_ℓ, which are defined by

$$f_\ell = \int_\ell d\ell \int_0^\infty d\nu \; G(\vec{r}, \nu) \; \epsilon(\nu) \tag{1}$$

where $G(\vec{r}, \nu)$ is the spectral emissivity of the plasma, $\epsilon(\nu)$ denotes the response of the filter/detector system and ℓ represents the line of sight. The chord brightness f is then equal to the power impinging on the detector divided by the throughput of the collimating aperture/detector combination. In general, the values of $\epsilon(\nu)$ are assumed to be equal for all lines of sight. Under these conditions, eq. (1) reduces to

$$f_\ell = \int_\ell d\ell \; g(\vec{r}), \qquad \ell = 1 \ldots n_\ell \tag{2}$$

with

$$g(\vec{r}) = \int_0^\infty d\nu \; G(\vec{r}, \nu) \; \epsilon(\nu). \tag{3}$$

The problem of tomography then consists of inverting the set of n_ℓ integral equations (2).

Therefore, the set of detectors should be as uniform as possible and have, up to a relative calibration factor, the same response for a given spectrum of incident radiation. An incorrect relative calibration can cause systematic errors in the tomographic reconstruction of the emissivity, resulting in artefacts which may obscure, or be mistaken for, features of interest. For normal incidence, a relative calibration by direct comparison of detector signals generated by a reference radiation source in the relevant spectral range is generally believed to be sufficient. The use of linear detector arrays on the other hand implies that each diode detects the X-rays under a different angle of incidence.

The aim of this work is to investigate the possibility of obtaining a precise relative calibration of pn-photodiodes which are used under varying angles of incidence.

In the next section, we present a method for calculating the photodiode efficiency as a function of the angle of incidence. The third section shows how these calculations, together with experiments using a commercial X-ray source, have been used to obtain a relative calibration of the photodiodes which will be used for X-ray tomography on the TCV tokamak, the 'Tokamak à Configuration Variable'. Finally, we apply our results to a set of simulated X-ray emission data.

2 Calculation of Photodiode Efficiencies

2.1 Modelling of the diode

The simplified geometry underlying our calculation of photodiode efficiencies is illustrated schematically in figure 2. The n-type Silicon substrate of thickness D is strongly doped near the front surface. The depletion zone of thickness V extends below this p^+ doped zone. The entire surface is covered by a passivation layer, for example by Si_3N_4. Apart from these purely geometric quantities, the efficiency is assumed to depend only on the diffusion length L_p of the minority carriers. The diffusion length again depends on the diffusion coefficient D_p and the carrier lifetime τ_p following $L_p = \sqrt{(D_p \tau_p)}$, where D_p is proportional to the mobility μ_p, following Einstein's relation $D_p = kT/e_0\mu_p$.

We assume that the thickness of the substrate, depletion zone and passivation layer are all known. The diffusion length as well as the thickness of the strongly doped layer are generally unknown *a priori* and are therefore treated as free parameters. Zero bias voltage will always be assumed in the following. The depletion zone and the bulk are considered as 'diode', whereas the p^+ zone and the passivation layer together with optional Beryllium foils in front of the detector are regarded as external filters.

To calculate the angular dependence of the efficiency with this essentially one-dimensional model, it is assumed that the diode extends infinitely in the plane parallel to the surface. Consequently, the thicknesses of the passivation layer, the p^+-zone, the depletion zone, the bulk and the diffusion length simply have to be multiplied by $1/\cos(\theta)$, where θ denotes the angle of incidence with respect to the surface normal, *i.e.* $\theta = 0^o$ means normal incidence. Unless stated otherwise, the thickness of the Be foil does not change with θ.

2.2 Diode Efficiency

The fraction of monochromatic radiation absorbed locally within a thin layer dx at a distance x from the surface is given by $\alpha \exp(-\alpha x)dx$, if $\alpha = \alpha(\nu)$ is the absorption coefficient of Silicon (units $1/m$), which depends on the photon energy. Let Φ_0 be the initial flux of photons of energy $h\nu$ (units $1/m^2 s$), E_{pn} the energy required to generate one electron-hole pair ($E_{pn} = 3.63eV$), e_0 the elementary charge and $p(x)$ the probability of detecting a charge generated at x, *i.e.* the probability that this charge reaches the depletion zone. The

total photoinduced current density is then given by

$$j = \Phi_0 h\nu \frac{e_0}{E_{pn}} \int_0^D \alpha \ \exp(-\alpha x)\ p(x)\ dx \tag{4}$$

The incident light intensity is $\Phi_0 h\nu$, which yields

$$r = \frac{e_0}{E_{pn}} \int_0^D \alpha \ \exp(-\alpha x)\ p(x)\ dx \tag{5}$$

for the responsivity r (units A/W). The integral can then be defined as the efficiency η.

$$\eta = \int_0^D \alpha \ \exp(-\alpha x)\ p(x)\ dx \tag{6}$$

Assuming that $p(x) = 1$ for a charge generated within the depletion zone of thickness V, $p(x) = \exp(-(x - V)/L_p)$ (see *e.g. Kingston* [2]) for $V < x \leq D$ and $p(x) = 0$ elsewhere, we obtain

$$\eta = 1 - \exp(-\alpha V) \times (1 - \frac{\alpha L_p}{1 + \alpha L_p}[1 - \exp(-(\alpha + 1/L_p)(D - V))]) \tag{7}$$

The efficiency η is a function of the photon energy ($\eta = \eta(\nu)$) because of the energy dependence of the absorption coefficient α. In the limit of an infinitely thick substrate ($D \to \infty$) η converges to

$$\eta_\infty = 1 - \frac{\exp(-\alpha V)}{1 + \alpha L_p} \tag{8}$$

an expression, which has also been obtained by *Sze* [3] from a solution of the continuity equation for the given set-up. Figure 3 shows the efficiency as a function of photon energy for two values of the diffusion length.

2.3 Spectrum averaged efficiency $< \eta >_\nu$

It is convenient to define a spectrum averaged efficiency, in the following denoted as $< \eta >_\nu$, which characterises the diode/filter combination for a given spectrum. Let $n(\nu)$ denote the number of incident photons per unit area, time and frequency interval (units $m^{-2}s^{-1}Hz^{-1}$), then $h\nu \times n(\nu) = w(\nu)$ is a spectral power distribution. The spectrum averaged photocurrent density j is then given by

$$j = \frac{e_0}{E_{pn}} \frac{\int \eta(\nu)\tau(\nu)w(\nu)d\nu}{\int w(\nu)d\nu} \tag{9}$$

where different filters of thickness d_i are taken into account using

$$\tau(\nu) = \prod_i \exp(-\alpha_i(\nu)d_i), \tag{10}$$

α_i and d_i denoting the absorption coefficient and the thickness of the corresponding filter material, respectively. This suggests using the following expression as a definition of $< \eta >_\nu$, the spectrum averaged efficiency

$$< \eta >_\nu = \frac{\int \eta(\nu)\tau(\nu)w(\nu)d\nu}{\int w(\nu)d\nu} \tag{11}$$

using $\eta(\nu)$ given above (equation (7)). $< \eta >_\nu$ multiplied by e_0/E_{pn} equals the photocurrent induced by $1W$ of radiation with a spectral distribution given by $w(\nu)$ impinging on the first filter.

2.4 Applications

The calculations presented here always refer to the geometric parameters of CENTRONIC's 5T-series diodes chosen for the TCV tomography system. From the capacitance per unit surface area given in the

data sheet [4], the thickness of the depletion zone can be estimated ($V \approx 3\mu m$). The substrate thickness is $D = 380\mu m$ [5]. The Si_3N_4 passivation layer of thickness $d_{Si_3N_4} = 55nm$ [5] is treated by decomposition into Si and N with appropriate equivalent thicknesses. The p^+ layer is assumed to consist entirely of Si, the dopant not being taken into account.

Two kinds of spectral distributions are considered: the X-ray spectrum of a hot thermal plasma and the spectrum of an electron beam X-ray source. In the case of X-ray emission from a plasma, an additional $47\mu mBe$ filter is included in the calculation, in the case of the Tungsten X-ray source a $125\mu mBe$ filter and $109mm$ of air, which is assumed to consist only of Nitrogen and Oxygen, are taken into account. (The latter parameters are those of our calibration experiment described in the following section). The effective thicknesses of Beryllium and air do not change with the angle of incidence. The data for the total photoabsorption cross section were taken from *Veigele* [6].

The spectral power distribution for a Hydrogen or Deuterium plasma is essentially a decaying exponential

$$w(\nu) = const \times \frac{1}{\sqrt{kT_e}} \exp(-h\nu/kT_e) \qquad (12)$$

where k is the Boltzmann constant and T_e is the electron temperature (see *e.g. Miyamoto* [7]). This distribution describes contributions from bremsstrahlung and recombination. The spectrum is also appropriate for a plasma contaminated with light impurities only ($Z \leq 8$) since the recombination edges are well below the low energy cutoff of the external filters. In practice, radiation incident on a diode consists of contributions from all along the line of sight which originate

from regions of different temperature. We therefore model the incident spectrum as a superposition of spectra from a plasma with an electron temperature distribution given by

$$T_e(r) = T_e(0)(1 - r^2)^p \quad (-1 < r < 1) \tag{13}$$

where $T_e(0)$ is the maximum temperature along the line of sight and p is the so-called peaking-factor, in the following $p = 1$. This shape is a reasonable fit to profiles seen in many fusion devices.

The Bremsstrahlung radiation of an electron beam source can be derived from a non-relativistic, but quantum-mechanical calculation given *e.g.* by *Jackson* [8]:

$$w_{brems}(\nu) = const \times \ln\left(\frac{(\sqrt{e_0 U_{xrs}} + \sqrt{e_0 U_{xrs} - h\nu})^2}{h\nu}\right) \tag{14}$$

U_{xrs} denotes the acceleration voltage. The spectral distributions used in the calculations are fits to experimental PHA spectra of an electron beam X-ray source with a tungsten anode, using $w_{brems}(\nu)$ from above and Gaussian profiles for the Tungsten lines. Figure 4 displays typical spectral distributions from an e^--beam X-ray source and a thermal plasma, filtered by $125\mu mBe$ and $47\mu mBe$, respectively.

Figures 5 ... 8 show some examples of $< \eta >_\nu$ as a function of angle of incidence and different values of the diffusion length L_p for the above mentioned sets of filters and different spectral distributions. The p^+ zone is assumed to be $0.5\mu m$ thick. The spectral distributions used to calculate $< \eta >_\nu$ contain the transmissions of the $47\mu mBe$-foil and the $125\mu mBe$-foil plus air, respectively. Therefore, $e_o/E_{pn} \times < \eta >_\nu$ equals the current induced by $1W$ of radiation of the given distribution impinging on the passivated diode surface.

In case of X-ray source spectra (figure 8) a large fraction of high energy photons is present, which results in a relatively large increase of efficiency with increasing θ. $< \eta >_\nu$ depends on U_{xrs}, L_p and on d_{p+}, which offers an opportunity to determine the unknown parameters from measurements of angular dependences of $< \eta >_\nu$. The angular dependence of $< \eta >_\nu$ on d_{p+} is much weaker for $30kV$ than for $10kV$ (see figure 9). The knowledge of the parameters L_p and d_{p+} then allows us to calculate $< \eta >_\nu$ for any given spectral distribution, which should represent a way to infer a relative calibration for any incident spectrum. Other results are discussed below (see section 4).

3 The Calibration Experiment

3.1 Set-up

The tomography system of the TCV tokamak is equipped with CENTRONIC's LD20-5T photodiodes. These are linear arrays of 20 n-type silicon pn-diodes. For use as X-ray detectors, the glass window was removed. The diode arrays are mounted on printed preamplifier circuit boards. The preamplifier transimpedance gain is $2.2 \times 10^5 V/A$ with a standard deviation of less than 0.6%. The detectors are used in photovoltaic mode, *i.e.* no bias is applied.

A schematic of the calibration experiment is shown in figure 10. A commercial electron beam X-ray source with a tungsten anode and a $125\mu m$ Be window is used (KEVEX PXS4). The voltage U_{xrs} and current I_{xrs} can be varied from $5kV$ to $30kV$ and from $0mA$ to $2mA$, respectively. Source spectra have been measured using a Germanium

detector and a PHA detection system with an energy resolution of $\approx 1keV$ FWHM in the energy range under consideration.

The diodes together with the preamplifier prints are mounted on a turntable, the rotational axis of which coincides with the surface of the diodes. The angle of incidence of the X-rays can be varied between -50^o and $+50^o$. The array position can be adjusted to allow identical conditions of irradiation for each of the 20 diodes of one array. The distance between the Be exit window of the source and the surface of the detectors is accurately known ($109mm$). A chopper with a $250\mu m$ thick steel wheel is inserted between the source and the detector. The resulting AC output voltage of the preamplifiers is detected by a 2-phase lock-in amplifier.

3.2 Experimental Procedure and Data Analysis

Simulations indicate that two sets of measurements ($U_{xrs} = 10kV$ and $U_{xrs} = 30kV$) at angles of 0^o and 50^o with a statistical error (standard deviation) of about 0.3% are sufficient to determine L_p and d_{p+} with a precision of about $\approx 5\%$ and $\approx 10\%$ respectively. The electron beam current of the source at $30kV$ was chosen to be much lower ($0.03mA$) than the current at $10kV$ ($1mA$) to irradiate with approximately equal power [9]. Under these conditions, the requirements on the statistical error of the output signal of the lock-in amplifier U_{out} were met. Measurements were performed at -50^o, 0^o and $+50^o$ to eliminate any possible offset in θ. The measurements took about $40min$ for each of

the 10 arrays of 20 diodes and each of the two applied voltages.

From the measured output signals U_{out} the experimental ratio

$$R_{exp} = \frac{U_{out}(50^o)}{U_{out}(0^o)\cos(50^0)} \tag{15}$$

was calculated for each detector and each of the two acceleration voltages ($10kV$ and $30kV$), the $\cos(\theta)$ factor representing the usual change of effective detector surface with θ.

Using the formulae given in section 2, tables of $< \eta >_\nu$ as a function of U_{xrs}, θ, L_p and the thicknesses d_i of the relevant external filters were generated for different p^+ layer thicknesses d_{p+}. From these tables the theoretical ratio

$$R_{theo}(L_p, d_{p+}) = \frac{< \eta >_\nu (U_{xrs}, \theta = 50^0, d_i, d_{p+}, L_p)}{< \eta >_\nu (U_{xrs}, \theta = 0^0, d_i, d_{p+}, L_p)} \tag{16}$$

was deduced. A preliminary estimate of L_p for each diode was obtained by looking up R_{exp} in the table of ratios $R_{theo}(L_p, d_{p+})$. From the individual values of L_p, an average value $\overline{L_p}$ was calculated for every array. The thickness of the p^+ zone d_{p+} was determined by finding the crossing point d^*_{p+} of the two functions $\overline{L_p}(d_{p+}, U_{xrs} = 30kV)$ and $\overline{L_p}(d_{p+}, U_{xrs} = 10kV)$ for every array. It was not possible to determine the dead layer thickness d_{p+} for every single diode because of the weak dependence of R on d_{p+} (see figure 9). The final individual values of L_p were then determined after a 2^{nd} iteration by using the value of d^*_{p+} thus obtained to recalculate $R_{theo}(L_p, d^*_{p+})$ and looking up R_{exp} in this table again. Because L_p is expected to vary slowly and continuously across the chip, a polynomial fit ($n = 2$) of L_p as a function of the diode number has finally been performed.

It has to be stressed here that the values of $< \eta >_\nu$ obtained from measurements of angular dependences are independent of any long-term fluctuations of the source or drifts in the electronics. Stability is only required for the several minutes necessary to record the output signals at three different angles for each detector. This means that a relative calibration relying on these data requires no absolute hardware reference.

In addition, the detector / preamplifier output U_{out} for a fixed X-ray source voltage ($30kV$) and normal incidence ($\theta = 0$) has been measured for all arrays within a period of $4h$. Within this time, a drift of the source/detector/electronics output of less than 1% was assured. The relative calibration thus obtained serves as a comparison to the relative calibration obtained by calculating $< \eta >_\nu$ from L_p and d_{p+}.

4 Results and Discussion

Figure 11 a) shows the 'raw' diffusion lengths L_p obtained by the table look-up for one of the arrays, together with a polynomial fit of degree 2. All values of the diffusion length obtained for the LD20-5T detectors investigated are very similar, *i.e.* $(200 \pm 20)\mu m$, in agreement with an estimation by the supplier CENTRONIC [5]. The mean value of the thickness of the p^+ layer varies from array to array between $0.6\mu m$ and $0.8\mu m$[1] with an error of $\approx \pm 0.1\mu m$.

In figure 11 b), relative values of $< \eta >_\nu$ calculated from the L_p-fit shown above are displayed for $\theta = 0, U_{xrs} = 30kV$. The relative

[1]The value of d_{p+} used in section 2.4 was chosen according to this result

values are obtained by dividing $< \eta >_\nu$ by $\overline{< \eta >_\nu}$, the average of diodes #2...#19. The first and the last detector of each array have a higher efficiency with respect to the inner diodes because of diffusion from the borders [5]. The difference is 5%, approximately independent of the spectral distribution of the incident radiation, which has been confirmed experimentally for the range of $U_{xrs} = 5kV$ to $U_{xrs} = 30kV$. A comparison with relative efficiencies from the 'direct' measurement is also shown ($\theta = 0, U_{xrs} = 30kV$). The standard deviation between these two independent sets of data is typically 0.5%, except for diodes # 1 and # 20. This means that a very precise detector-to-detector calibration can be obtained by the calculation of $< \eta >_\nu$ from L_p and d_{p+}.

In figure 11 c), relative values of $< \eta >_\nu$ calculated from the L_p-fit for radiation from a plasma are displayed ($kT_e(0) = 1, 5$ and $10keV$). Comparison shows that a simple application of relative calibration factors obtained from a direct measurement ($\theta = 0$ only) with an electron beam X-ray source to radiation from a plasma may not be adequate for lower temperatures: Relative calibration factors of $\approx 0.98 \ldots 1.01$ measured with the X-ray source at $30kV$ are reduced to $\approx 0.998 \ldots 1.001$ in the case of $kT_e(0) = 1keV$. With increasing $kT_e(0)$, the differences increase because of an increasing fraction of high energy photons (see figure 11 c)).

The thickness of the dead layer is assumed to be the same for all diodes of a single array for reasons given in the previous section. However, its influence *should* be apparent in the array-to-array calibration: figure 12 a) shows relative values of $< \eta >_\nu$ for the X-ray

source, $U_{xrs} = 30kV$, calculated from L_p and d_{p+} for the entire set of 10 arrays (continuous curve). A correction of 5% for the first and the last diode of each array is included. The open circles represent the second independent set of measurements mentioned in the preceding section ($\theta = 0, U_{xrs} = 30kV$, measured all within $4h$). The relative value is again obtained by dividing $< \eta >_\nu$ by the average $\overline{< \eta >_\nu}$ over all diodes, except for diode # 1 and # 20 of each array. The maximum difference between the two data sets is 3.5%, the standard deviation is 1.2%, *i.e.* in this case a relative array-to-array calibration with an accuracy of $\approx 2\%$ is provided (see part b) of figure 12).

It is essentially the presence of the dead layer which limits the precision of the relative calibration for radiation from a plasma: compared to radiation from an electron beam X-ray source a much larger fraction of low energy photons which are absorbed near the surface is present. For normal incidence, $< \eta >_\nu$ drops exponentially with increasing d_{p+}: $< \eta(d_{p+}) >_\nu \approx < \eta(0) >_\nu \times \exp(-\beta d_{p+})$ where $\beta = 0.0638\mu m^{-1}$ for $U_{xrs} = 30kV$ and $\beta = 0.285\mu m^{-1}$ for $kT_e(0) = 1keV$, which means that 1% error due to variations of d_{p+} in the first case corresponds to 4% in the latter.

The angular dependence of $< \eta >_\nu$ for $kT_e(0) = 0.3, 1, 5$ and $10keV$ is displayed in figure 6 for the case of a $47\mu m$ thick, curved Be foil : For $L_p = 200\mu m$ and $d_{p+} = 0.5\mu m$, the ratio $< \eta(60^o) >_\nu$ / $< \eta(0^o) >_\nu$ increases from 0.89 at $kT_e(0) = 0.3keV$ to ≈ 1.07 at $kT_e(0) = 10keV$. This implies that a relative calibration from a measurement only at zero angle of incidence assigned to a detector facing these conditions may be wrong by 18%, unless some form of T_e-dependent correction

is performed. To assure a precision of 3% in the relative calibration of our LD20-5T arrays, the angle of incidence θ should not exceed 30^o for plasma temperatures of $T_e(0) \approx 1keV$ or lower.

Although these restrictions are already severe, it should be noted that the situation is even worse if the effective Be-foil thickness, too, depends on the angle of incidence. The ratio $< \eta(60^o) >_\nu \; / \; < \eta(0^o) >_\nu$ is displayed in figure 7 for $kT_e(0) = 0.3, 1, 5$ and $10keV$ and a flat Be-foil with a thickness of $47\mu m$. For $kT_e(0) = 1keV$ *e.g.* $< \eta >_\nu$ drops to 55% of its value at normal incidence as θ approaches 60^o. This is essentially due to the increase in apparent foil thickness as $1/cos(\theta)$. The use of curved Be-foils as on the Alcator-C-MOD tokamak [10] or on TCV appears to be necessary to avoid an excessive angular and spectral dependence of the filter/diode efficiency.

It should also be noted that these considerations are strictly correct only if all detectors are exposed to the same spectral distribution, which is not generally true: On large machines such as the JET tokamak, the maximum temperature on a viewing chord may be anywhere between $300eV$ and $12keV$. This means that more than a calibration in the usual sense (just constant calibration factors) is needed. To improve the accuracy, calibration factors could be corrected by calculating the spectral distribution for every line of sight, using the shape of the plasma (*e.g.* from magnetic diagnostics) and a temperature profile. This is unfortunate since data from tomography systems using flat arrays, unlike their predecessors based on individual detectors, cannot be inverted independently of other diagnostic data. Also, integrating these data is likely to be very complicated, though probably feasible,

as explained in the following section.

5 Simulation

To investigate a realistic case, we selected one of the detector arrays of the future TCV tomography system. Incidence angles span a range from 0^o to 50^o. The T_e-distribution was determined with the help of the magnetic flux contours and profiles of an ohmically heated discharge of TCV obtained from an equilibrium reconstruction code. The so-called peaking-factor was set to one and a central temperature of $1keV$ was chosen, which corresponds approximately to the experimental situation. The density profile of the purely hydrogenic plasma was assumed to be flat. Spectral distributions were then calculated for every line of sight, where an equal Be-foil thickness of $47\mu m$ for all detectors was taken into account.

The emissivity in the spectral region defined by the transmission of the Be-foil,

$$\tilde{g}(\vec{r}) = \int_0^\infty d\nu \; G(\vec{r}, \nu) \; \tau_{Be}(\nu) \tag{17}$$

is shown as a contour plot in figure 13 a), together with the TCV vessel wall, the plasma boundary and the lines of sight #1 ... #20.

Two sets of line-integrated data or chord brightnesses were then generated. One, in the following denoted as f_ℓ^1, by assuming equal response of the detectors $\eta(\nu) = 1$ for all frequencies, which is equivalent to inserting $\epsilon(\nu) = \tau_{Be}(\nu)$ in equation (1). The second set, f_ℓ^η, by taking into account the different angles of incidence θ_ℓ to calculate efficiencies $\eta(\nu, \theta_\ell)$ according to equation (7), where $L_p = 200\mu m$ and

$d_{p^+} = 0.5\mu m$ for all detectors of the LD20-5T-array. This means $\epsilon(\nu)$ in eqn.(1) is equal to $\tau_{Be}(\nu) \times \eta(\nu, \theta_\ell)$. Both sets of data are displayed in figure 13 b).

f_ℓ^1 was corrected by using the spectrum averaged efficiency from equation (11). $< \eta_\ell >_\nu$ was calculated taking into account the different angles of incidence θ_ℓ, but assuming the *same* spectral distribution with $kT_e(0) = 1keV$ and a $47\mu mBe$-filter for *all* lines of sight. Care has to be taken regarding the choice of the spectral distribution $w(\nu)$: To be consistent with the calculations of f_ℓ above, it has to be

$$w(\nu) = const \times \tau_{Be}(\nu) \times \int_{-1}^{1} dr \; \frac{exp(-h\nu/kT_e(r))}{\sqrt{kT_e(r)}} \qquad (18)$$

with $T_e(r)$ as given by equation (13), (see also eqn. (12) and (17)).

The result of this correction $f_\ell^{corr} = f_\ell^1 \times < \eta_\ell >_\nu$ is also displayed in figure 13 b) as the open circles. In figure 13 c) the relative differences between f_ℓ^{corr} and f_ℓ^η are shown. As was already evident from figure 13 b), the agreement between f^{corr} and f^η is excellent, in spite of the rather coarse approximation of the 'real' spectral distribution used to obtain $< \eta_\ell >_\nu$. Calculations with higher central temperatures $T_e(0)$ indicated that the quality of the correction provided by $< \eta >_\nu$ decreases slightly for $kT_e(0) > 2keV$.

As a result, we see that the relative error introduced by a failure to consider the angular dependence of the diode efficiency can be reduced significantly, at least at moderate temperatures, if spectrum averaged efficiencies for a 'standard' distribution with the central temperature are used as a correction.

6 Summary and Conclusion

We have shown that the response of Silicon pn-photodiodes to soft-X-rays can be adequately described in terms of a small set of parameters. The diffusion length of the minority carriers L_p and the thickness d_{p+} of the strongly doped zone below the front surface are of crucial importance. These parameters can be deduced from measurements of the angular dependence of the photoinduced current, provided that the spectral distribution of the incident radiation is known. The response of the diodes to any spectral distribution can then be calculated , which represents a very convenient way to obtain relative calibration factors.

The method has been applied to CENTRONIC LD20-5T detectors, linear arrays of 20 Silicon pn-photodiodes, which equip the pinhole cameras of the soft-X-ray tomography system on the TCV tokamak. The parameters L_p and d_{p+} have been determined using radiation from an electron beam X-ray source. For normal incidence, the precision of the relative detector-to-detector calibration within each array is typically 0.5%, the precision of the array-to-array calibration is $\approx 2\%$.

The geometry of the tomography set-up implies that the angle of incidence as well as the spectral distribution of the radiation is different for every single diode. In addition, unless a properly curved foil is used, the apparent thickness of the Be foil, which is used to block off visible light, is different for every detector. Using the specifications of LD20-5T, we have calculated the spectrum averaged efficiency $< \eta >_\nu$ for radiation from a hot thermal plasma, including the considerations

listed above. Even if the spectral distribution and the Be foil thickness are the same for all detectors, the presence of a dead layer several tenths of a μm thick forces us to restrict the angle of incidence θ: to assure a precision of relative response of 3% for $kT_e(0) = 1keV$, θ should not exceed 30^o. Under the same conditions ($kT_e(0) = 1keV$), the use of a flat Be-foil at angles of incidence of 0^o and 30^o already leads to a 10% difference in the relative response. In addition, the relative calibration depends on the temperature and density distribution on each line of sight. This means that more than just a constant calibration factor is needed if planar arrays of photodiodes are to be used for soft-X-ray tomography. A simple way to address this problem is the use of the spectrum averaged efficiency as a correction. We have shown that for $kT_e(0) = 1keV$, corresponding to typical ohmically heated plasmas in TCV, this correction significantly reduces the relative error, even if the spectrum of the incident radiation is assumed to be the same for all diodes. Such a correction will be adequate for TCV plasmas with central electron temperatures up to $2 - 3keV$, as expected with additional electron cyclotron heating. For higher temperatures, hardware modifications such as a reduction of the range of angles to $|\theta| < 30^o$, will be necessary.

Acknowledgments

We gratefully acknowledge fruitful discussions with *Roland Payne* from CENTRONIC as well as the communication of the specifications of the LD20-5T arrays. Thanks are also due to *Thierry Buchillier* and the 'Institut de Radiophysique Appliquée', Lausanne, for providing PHA spectra of our X-ray source. This work was partly supported by the *Swiss National Science Foundation.*

References

[1] *CAMACHO, J. F. and GRANETZ, R. S.:* Rev. Sci. Instrum **57** (1986) 417

[2] *KINGSTON, R.H.:* 'Detection of Optical & Infrared Radiation' Springer, Berlin/New York (1978)

[3] *SZE, S. M.:* 'Physics of Semiconductor Devices', 2nd ed. Wiley, New York (1981)

[4] *CENTRONIC*, main catalogue

[5] *CENTRONIC*, private communication

[6] *VEIGELE, W. M. J.:* Atomic Data **5**, No. 1 (1973)

[7] *MIYAMOTO, K.:* 'Plasma Physics for Nuclear Fusion',MIT Press (1976)

[8] *JACKSON, J. D.:* 'Klassische Elektrodynamik', de Gruyter, Berlin/New York (1981)

[9] *POHL, R. W.:* 'Optik und Atomphysik' 13. Auflage, Springer, Berlin/New York (1976)

[10] *GRANETZ, R. S., WANG, L.:* 'Design of the X-ray tomography system on Alcator C-MOD' in: ISPP9 "Piero Caldirola", Varenna Workshop on 'Diagnostics for Contemporary Fusion Experiments', P.E. Stott, D. K. Akulina, G. Gorini and E. Sindoni (Eds.) SIF Bologna (1991)

Figure 1: Principle scheme of the pinhole cameras used for soft-X-ray tomography on the TCV tokamak.

Figure 2: Geometry underlying our calculations of photodiode efficiencies: Thickness of the substrate D, width of the depletion zone V and the passivation layer thickness are assumed to be known. The thickness of the p^+ layer and the diffusion length are parameters. If not otherwise stated, the thickness of the Be-foil is kept constant for different angles of incidence θ.

Figure 3: The efficiency $\eta(\nu)$ of a Si-photodiode passivated by $55nmSi_3N_4$ with a dead layer of $d_{p^+} = 0.5\mu m$ is shown as a function of the photon energy in keV for $L_p = 200\mu m$ (solid curve) and $L_p = 1000\mu m$ (dash-dotted curve)

Figure 4: Spectral power distribution $w(\nu)$ in arbitrary units for radiation from an W-anode e^--beam X-ray source at $U_{xrs} = 30kV$ filtered by $125\mu m$ of Be (solid curve, fit to experimental data) and from a thermal plasma with a maximum electron temperature $kT_e(0) = 1keV$ filtered by $47\mu m$ of Be (dashed curve).

Figure 5: Spectrum averaged efficiency $< \eta >_\nu$ as a function of the diffusion length L_p. ++++ : for the case of the W-X-ray source, $w(\nu)$ is the spectral distribution *after* passing $125\mu mBe$. The other curves show $< \eta >_\nu$ for plasma radiation. Again, $w(\nu)$ is the distribution *after* filtering by $47\mu mBe$. The dotted, dashed, dash-dotted and solid curves correspond to $kT_e(0) = 0.3, 1, 5$ and $10keV$, respectively.

Figure 6: $< \eta(\theta) >_\nu / < \eta(0^o) >_\nu$ for radiation from a plasma, $L_p = 200\mu m$, $d_{p+} = 0.5\mu m$ and a curved Be-foil ($47\mu m$). The dotted, dashed, dash-dotted and solid curves correspond to $kT_e(0) = 0.3, 1, 5$ and $10keV$, respectively.

Figure 7: $< \eta(\theta) >_\nu / < \eta(0^o) >_\nu$ for radiation from a plasma, $L_p = 200\mu m$, $d_{p+} = 0.5\mu m$ and a 'flat' Be-foil ($47\mu m$), *i.e.* the apparent thickness varies as $1/\cos(\theta)$. The dotted, dashed, dash-dotted and solid curves correspond to $kT_e(0) = 0.3, 1, 5$ and $10keV$, respectively.

Figure 8: $< \eta(\theta) >_\nu / < \eta(0^o) >_\nu$ for radiation from an e^--beam W- X-ray source as a function of the angle of incidence θ for $L_p = 200\mu m$ (solid) and $L_p = 1000\mu m$ (broken). a): $U_{xrs} = 10kV$ b): $U_{xrs} = 30kV$

Figure 9: Ratio $R = < \eta(50^o) >_\nu / < \eta(0^o) >_\nu$ as a function of the diffusion length L_p for radiation from an e^--beam W- X-ray source, a) $U_{xrs} = 10kV$ and b) $U_{xrs} = 30kV$. Continuous curve: $d_{p+} = 0$, broken curve: $d_{p+} = 1\mu m$

Figure 10: Experimental set- up. Current I_{xrs} and Voltage U_{xrs} of the Tungsten electron beam X-ray source can be varied between $0-2mA$ and $5-30kV$, respectively. X-rays are filtered by $125\mu m$ of Be and $108.9mm$ of air, pass through a chopper with a $250\mu m$ steel wheel and hit the diode at an angle θ between 0^o and $\pm 50^o$. The axis of rotation, indicated by $\otimes$, coincides with the detector surface. The photocurrent is preamplified (I/U conversion) and then fed to a lock-in amplifier.

Figure 11: a): L_p from measurements of angular dependences of U_{out} for the 20 diodes of array # 4, open circles represent the values obtained by the table look-up. The solid curve is a polynomial fit (n=2) to the data. b): $< \eta >_\nu / \overline{< \eta >_\nu}$ calculated from the fit to L_p (solid curve) compared to the relative signal amplitudes from a 'direct' measurement ($\theta = 0, U_{xrs} = 30kV, d_{Be} = 125\mu m$, indicated by the $*$). Further explanations see text. c): $< \eta >_\nu / \overline{< \eta >_\nu}$ calculated from the same fit to L_p for radiation from a plasma. The curves correspond to $kT_e(0) = 1,5$ and $10keV$.

Figure 12: a): $< \eta >_\nu / \overline{< \eta >_\nu}$ obtained from L_p and d_{p+} for all arrays (solid curve) compared to an independent measurement of the relative efficiency using the X-ray source ($U_{xrs} = 30kV$ (open circles)). The reference value is in both cases the average over all diodes except for # 1 and # 20 of each array. b): Difference between the two data sets in percent

Figure 13: a): geometry of the TCV vessel and one of the X-tomo cameras. The plasma boundary (broken curve) and a contour plot of the emissivity calculated from an equilibrium reconstruction for TCV shot # 6764 at time $t = 0.28s$ are also shown. b): chord brightness f_ℓ as a function of the diode number ℓ. Solid: f_ℓ^η, taking into account the actual spectral distribution and $\eta(\nu, \theta_\ell)$ with the actual angle of incidence; broken: f_ℓ^1, assuming an ideal detector ,*i.e.* $\eta = 1$, open circles: correction $f_\ell^1 \cdot < \eta_\ell >_\nu$ using the spectrum averaged efficiency for the actual angle of incidence but assuming the *same* spectral distribution for all lines of sight. The corresponding relative deviations in percent are shown in c).

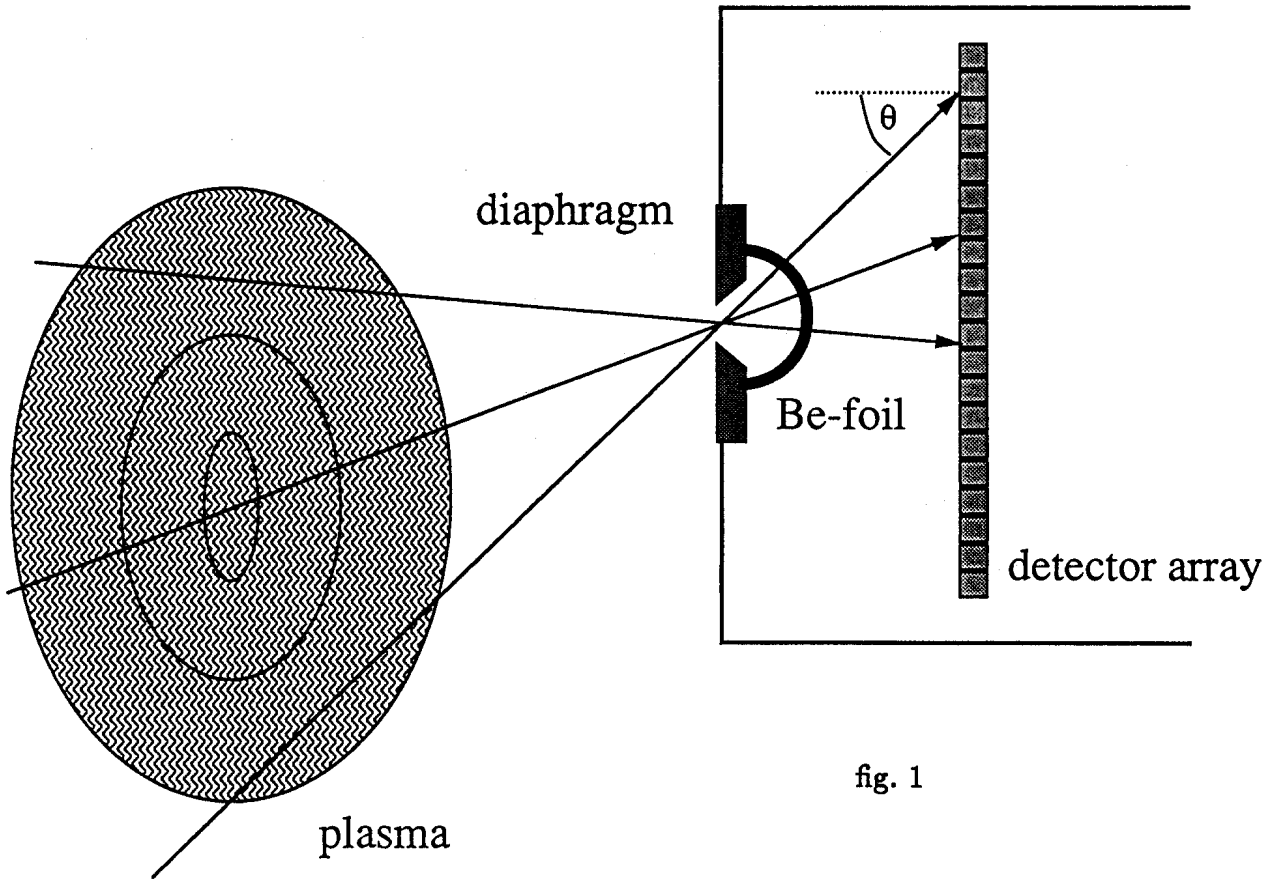
θ
diaphragm
Be-foil
detector array
plasma

fig. 1

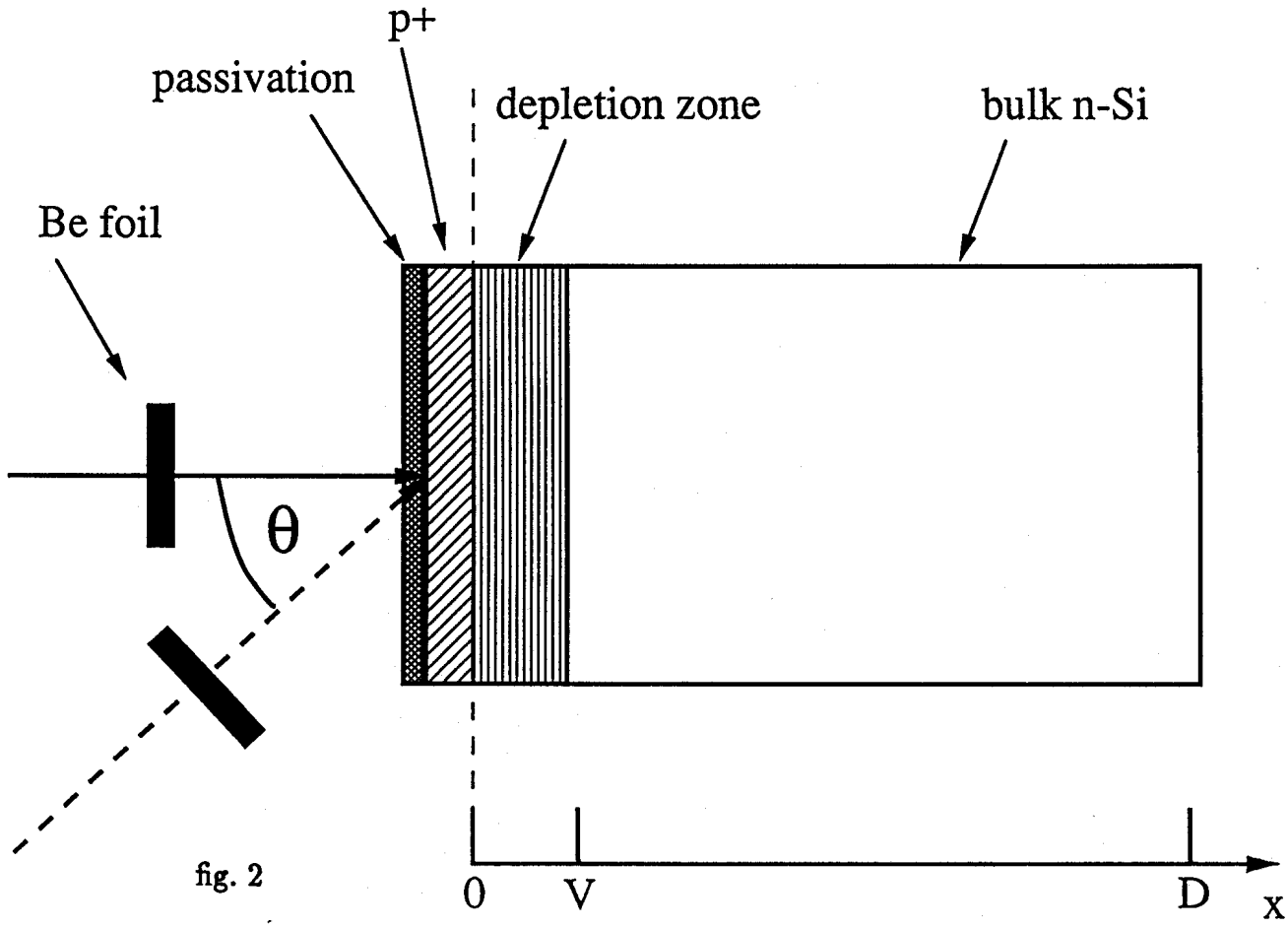
p+
passivation
depletion zone
bulk n-Si
Be foil
θ
0
V
D
x

fig. 2

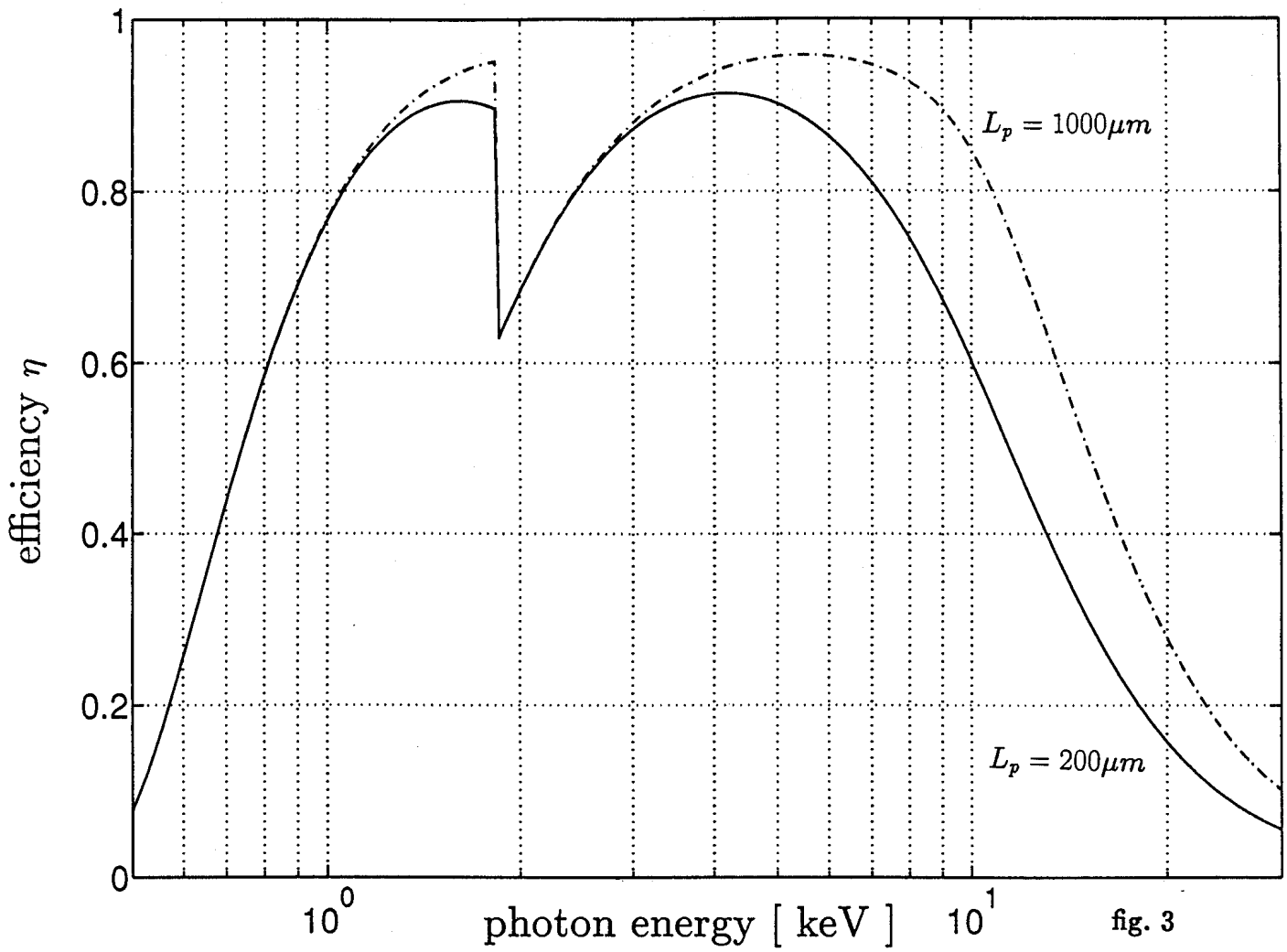
efficiency η
1
0.8
0.6
0.4
0.2
0
$L_p = 1000\mu m$
$L_p = 200\mu m$
10^0
10^1
photon energy [keV]

fig. 3

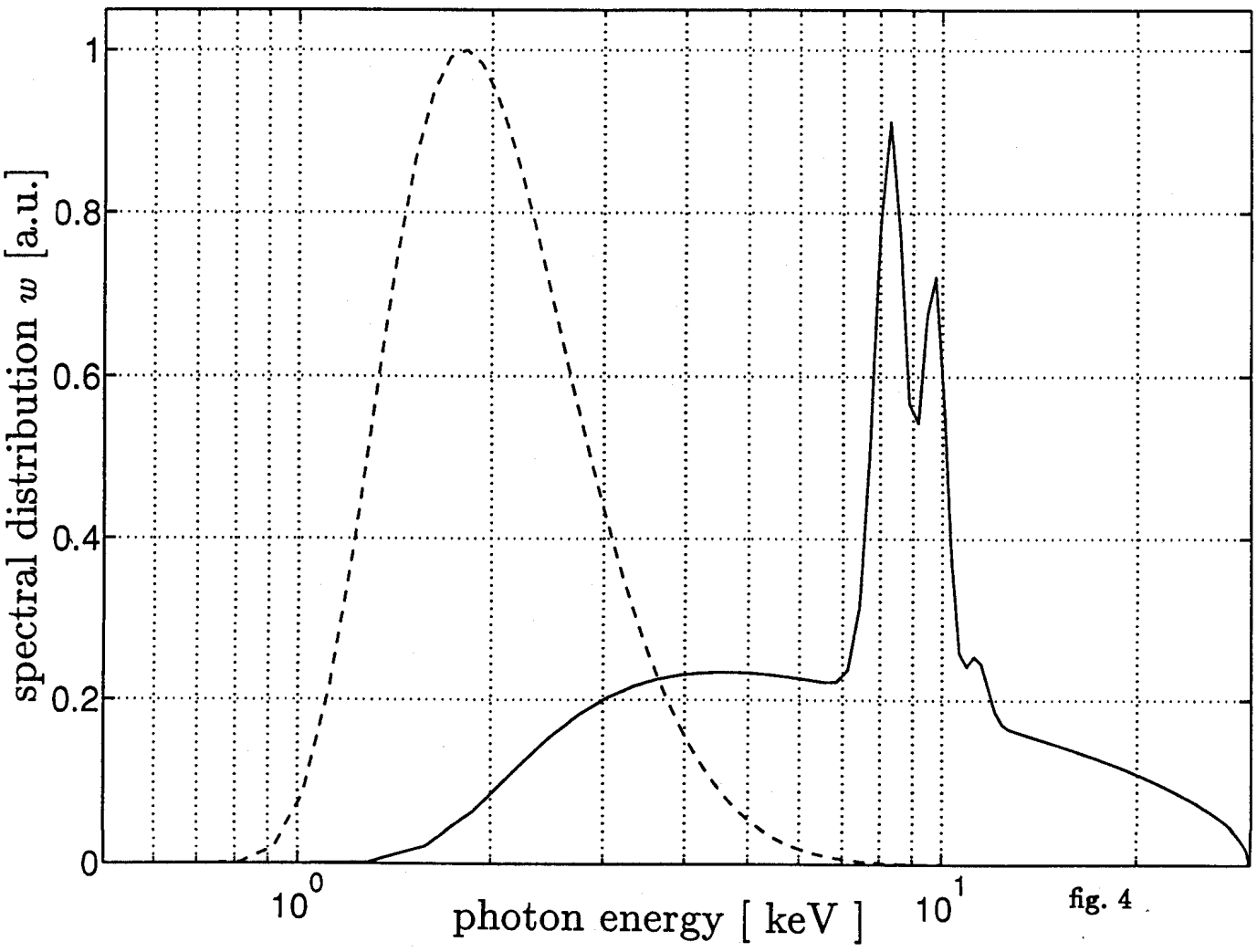
spectral distribution w [a.u.]
1
0.8
0.6
0.4
0.2
0
10^0
10^1
photon energy [keV]

fig. 4

fig. 5

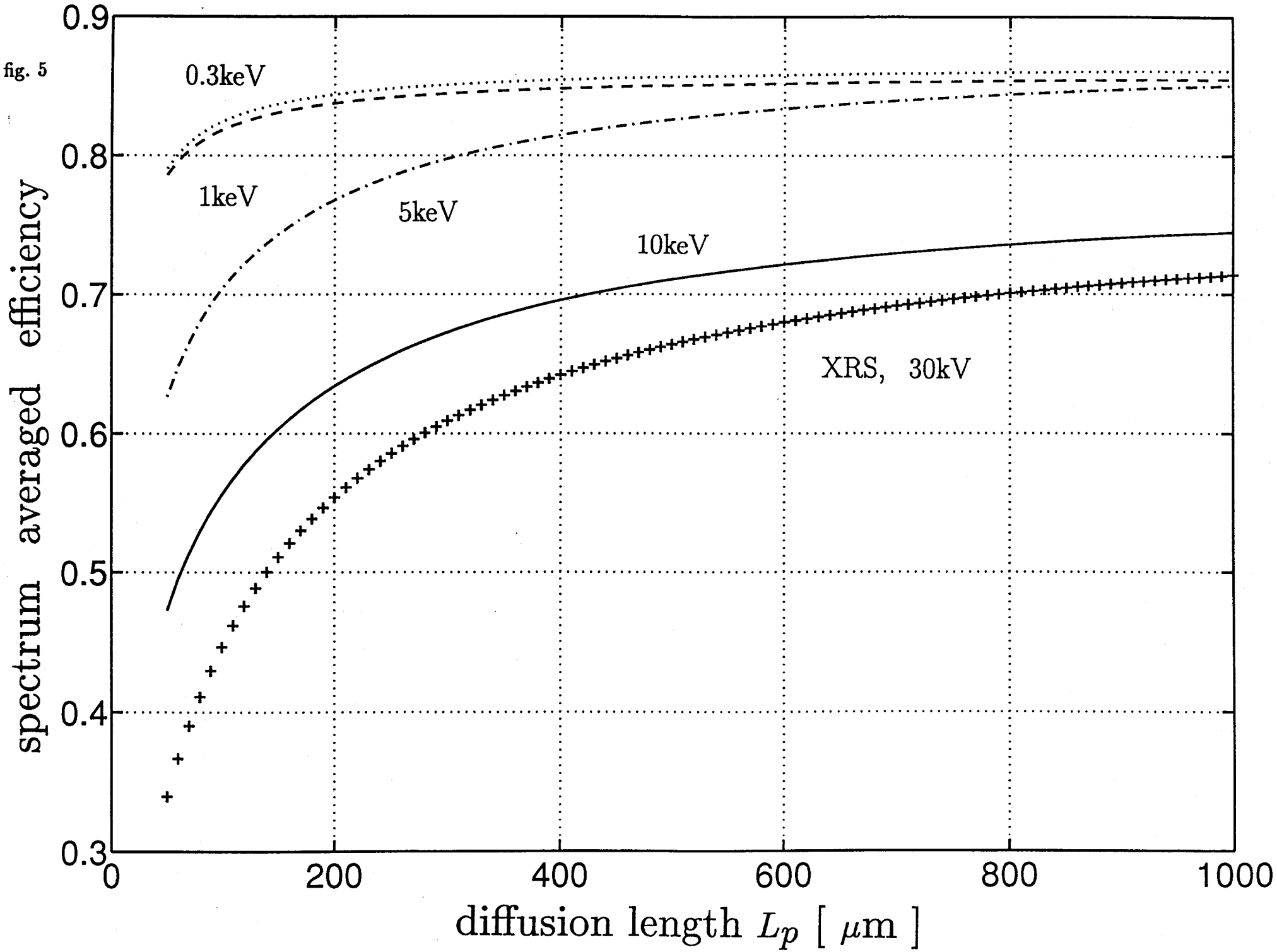
0.9
0.8
0.7
0.6
0.5
0.4
0.3
0
200
400
600
800
1000
spectrum averaged efficiency
diffusion length L_p [μm]
0.3keV
1keV
5keV
10keV
XRS, 30kV

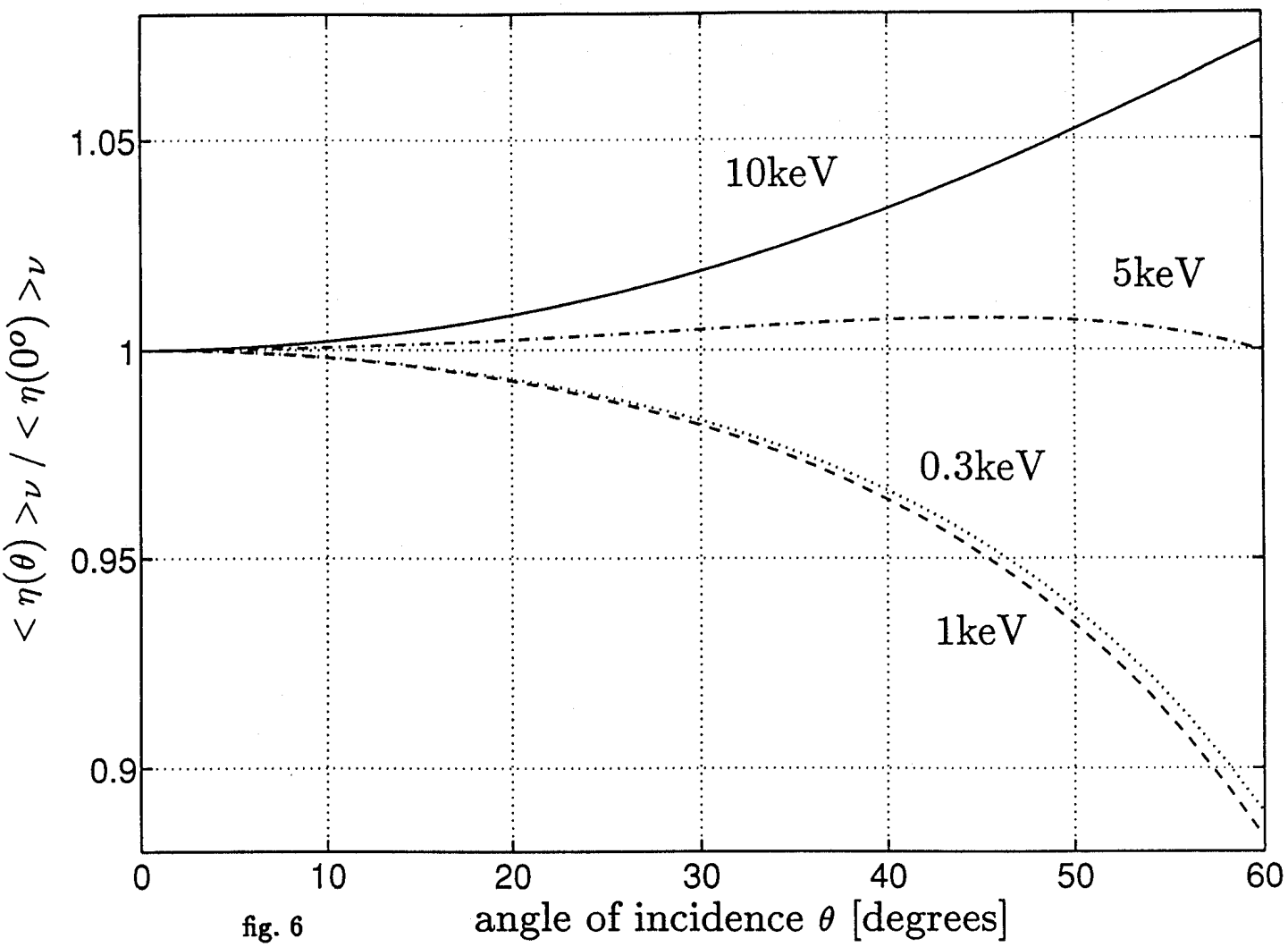
1.05
1
0.95
0.9
0
10
20
30
40
50
60
10keV
5keV
1keV
0.3keV
$< \eta(\theta) >_\nu / < \eta(0^o) >_\nu$
angle of incidence θ [degrees]

fig. 6

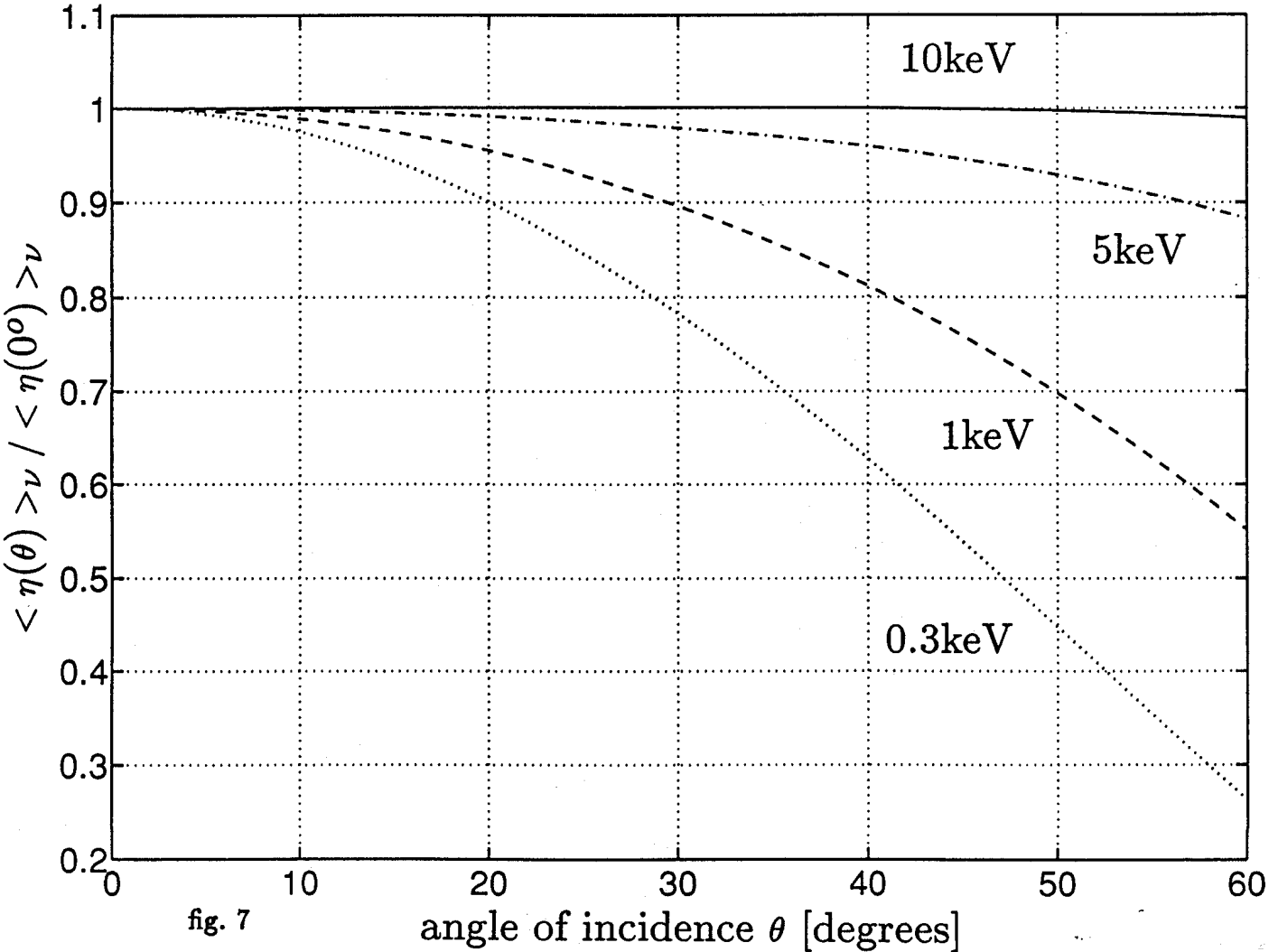
1.1
1
0.9
0.8
0.7
0.6
0.5
0.4
0.3
0.2
0
10
20
30
40
50
60
10keV
5keV
1keV
0.3keV
$< \eta(\theta) >_\nu / < \eta(0^o) >_\nu$
angle of incidence θ [degrees]

fig. 7

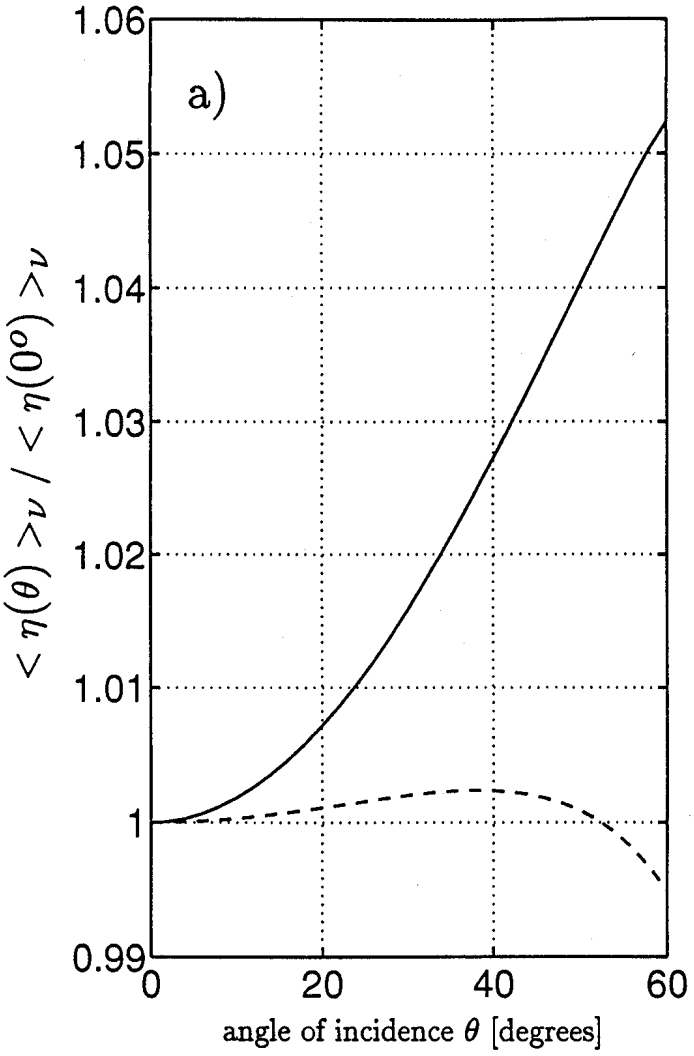
a)
1.06
1.05
1.04
1.03
1.02
1.01
1
0.99
0
20
40
60
$< \eta(\theta) >_\nu / < \eta(0^o) >_\nu$
angle of incidence θ [degrees]

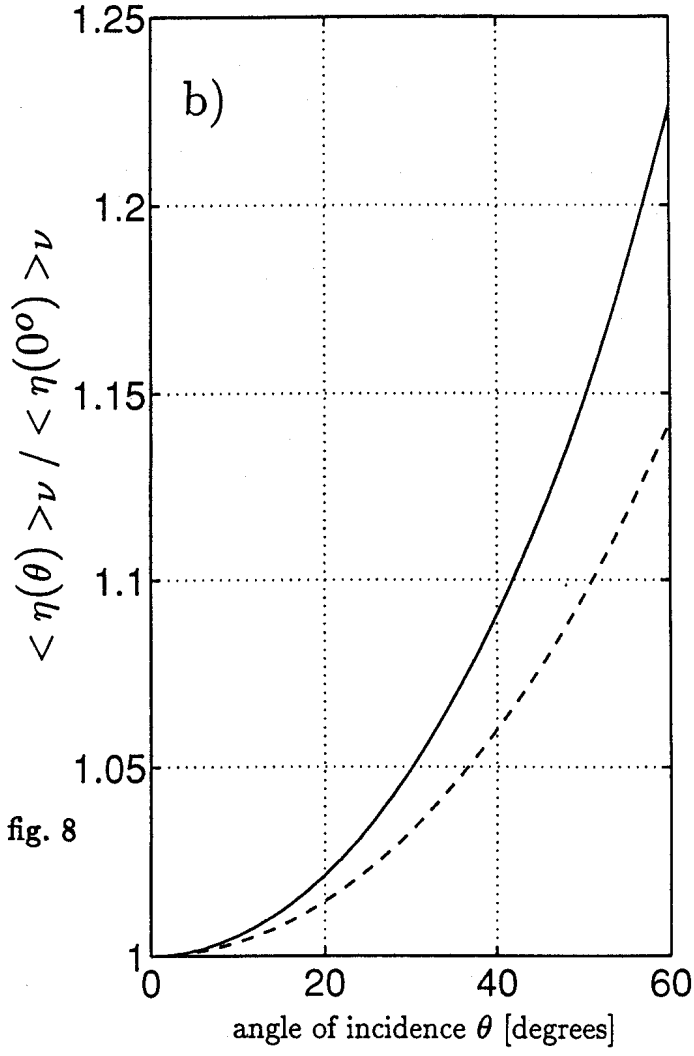
b)
1.25
1.2
1.15
1.1
1.05
1
0
20
40
60
$< \eta(\theta) >_\nu / < \eta(0^o) >_\nu$
angle of incidence θ [degrees]

fig. 8

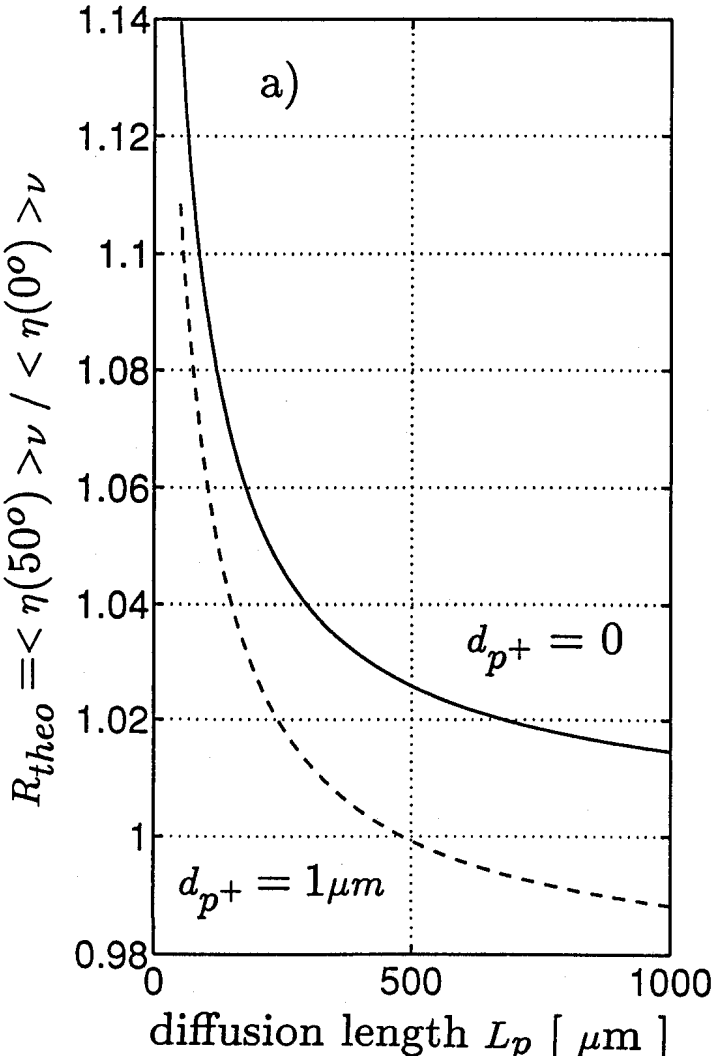
a)
1.14
1.12
1.1
1.08
1.06
1.04
1.02
1
0.98
0
500
1000
$R_{theo} = < \eta(50^o) >_\nu / < \eta(0^o) >_\nu$
$d_{p^+} = 0$
$d_{p^+} = 1\mu m$
diffusion length L_p [μm]

fig. 9

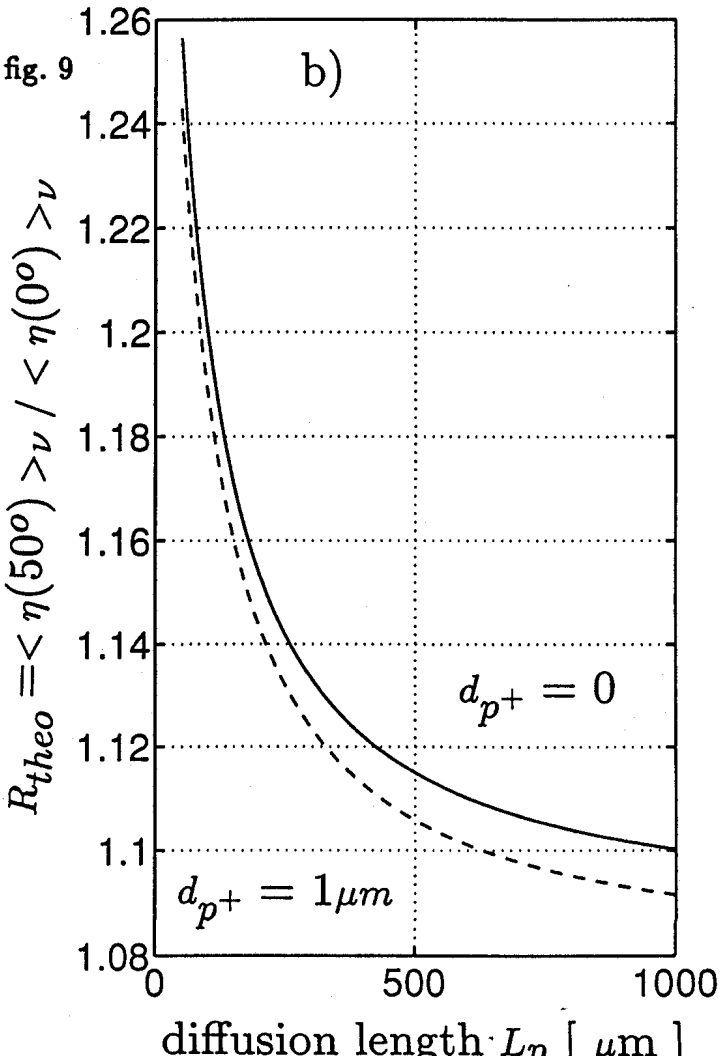
b)
1.26
1.24
1.22
1.2
1.18
1.16
1.14
1.12
1.1
1.08
0
500
1000
$R_{theo} = < \eta(50^o) >_\nu / < \eta(0^o) >_\nu$
$d_{p^+} = 0$
$d_{p^+} = 1\mu m$
diffusion length L_p [μm]

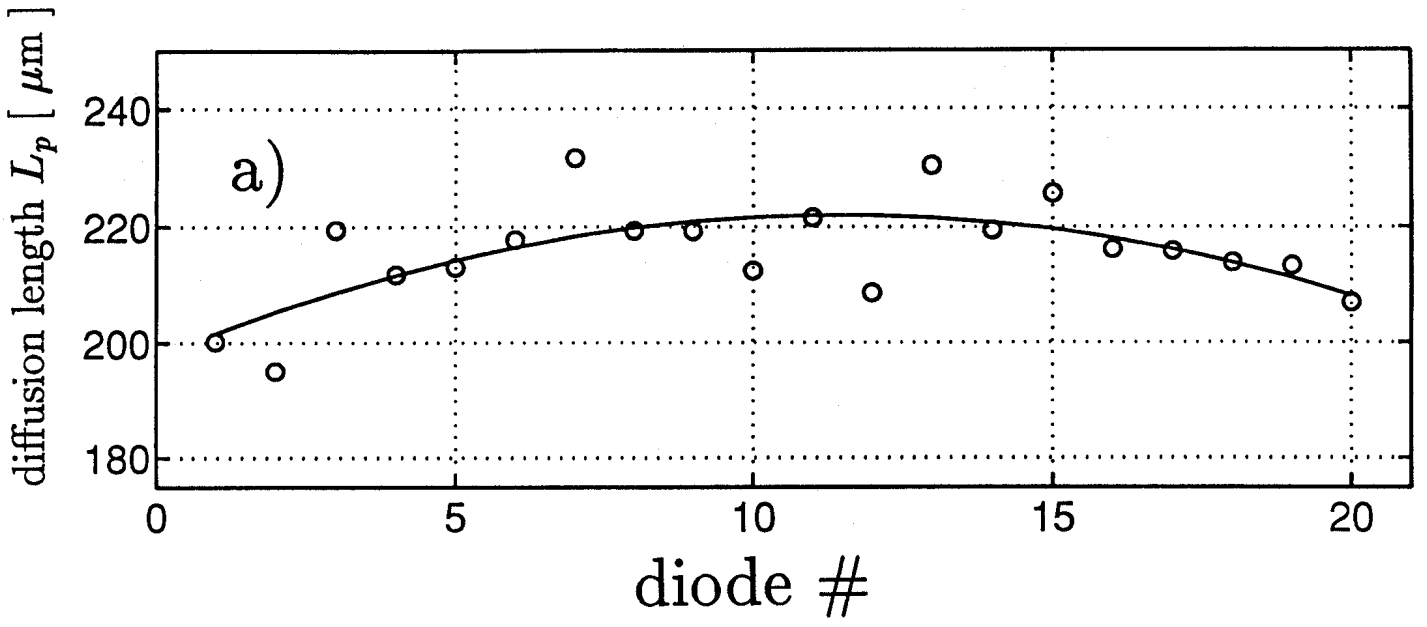
diffusion length L_p [μm]
240
220
200
180
a)
0
5
10
15
20
diode #

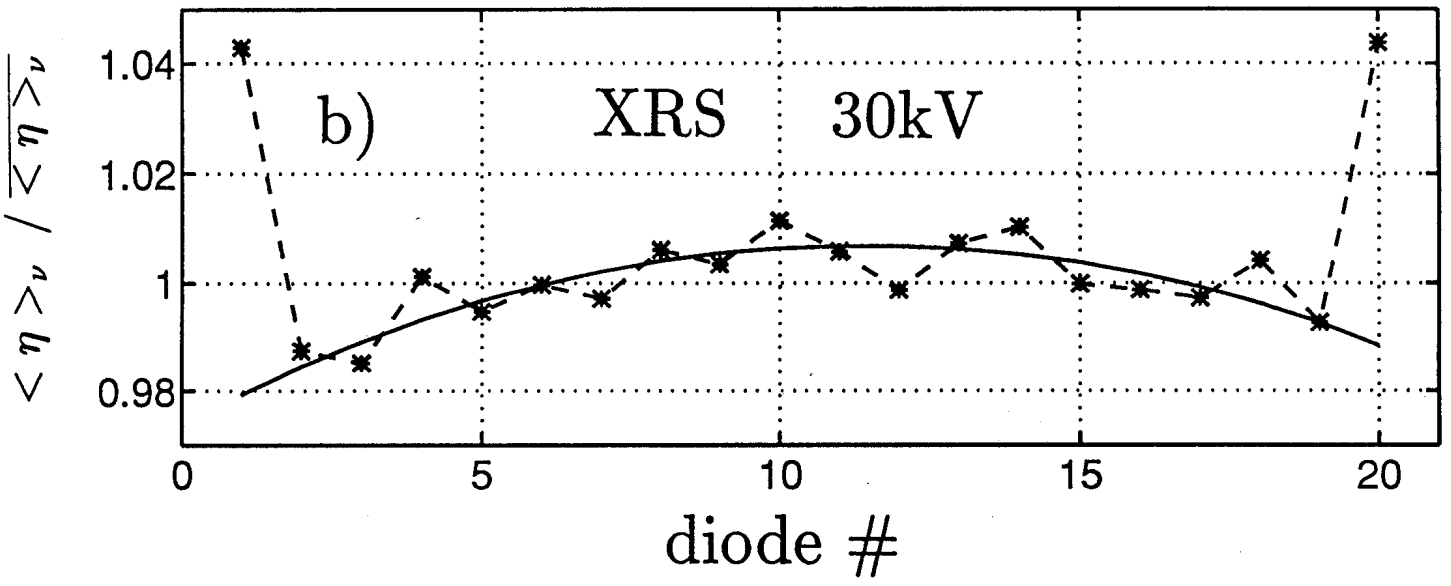
$< \eta >_\nu \; / \; \overline{< \eta >_\nu}$
1.04
1.02
1
0.98
b)
XRS
30kV
0
5
10
15
20
diode #

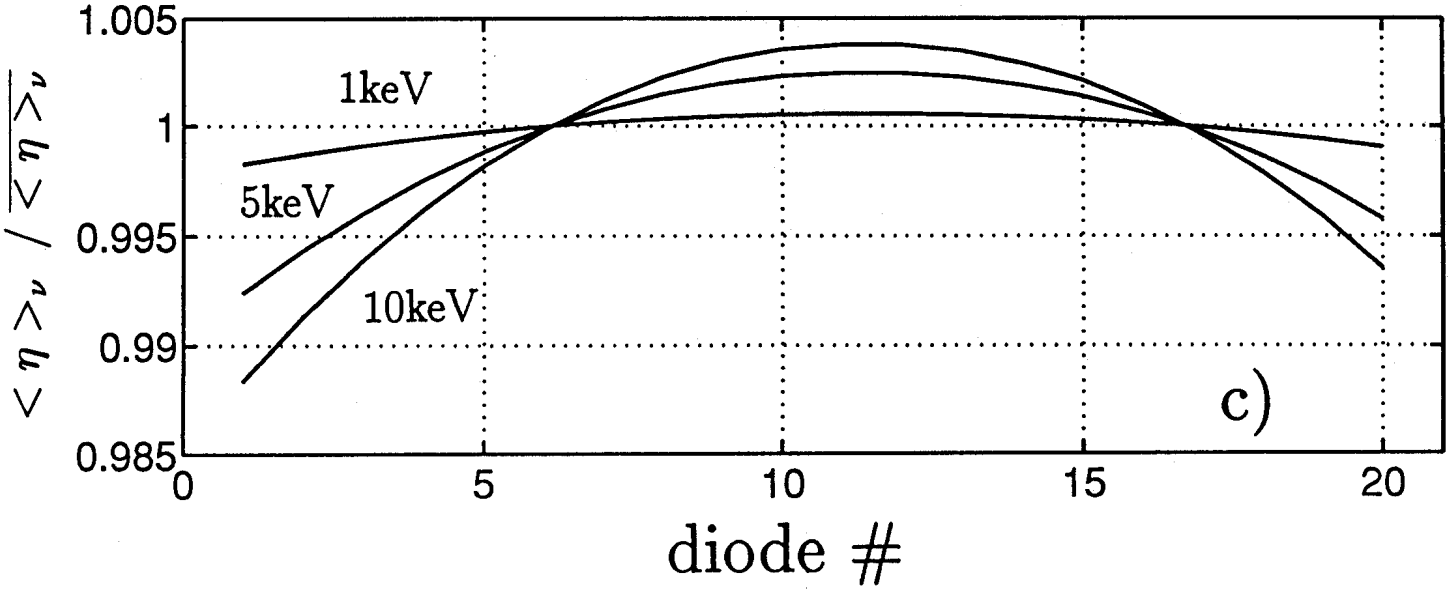
$< \eta >_\nu \; / \; \overline{< \eta >_\nu}$
1.005
1
0.995
0.99
0.985
1keV
5keV
10keV
c)
0
5
10
15
20
diode #

fig. 11

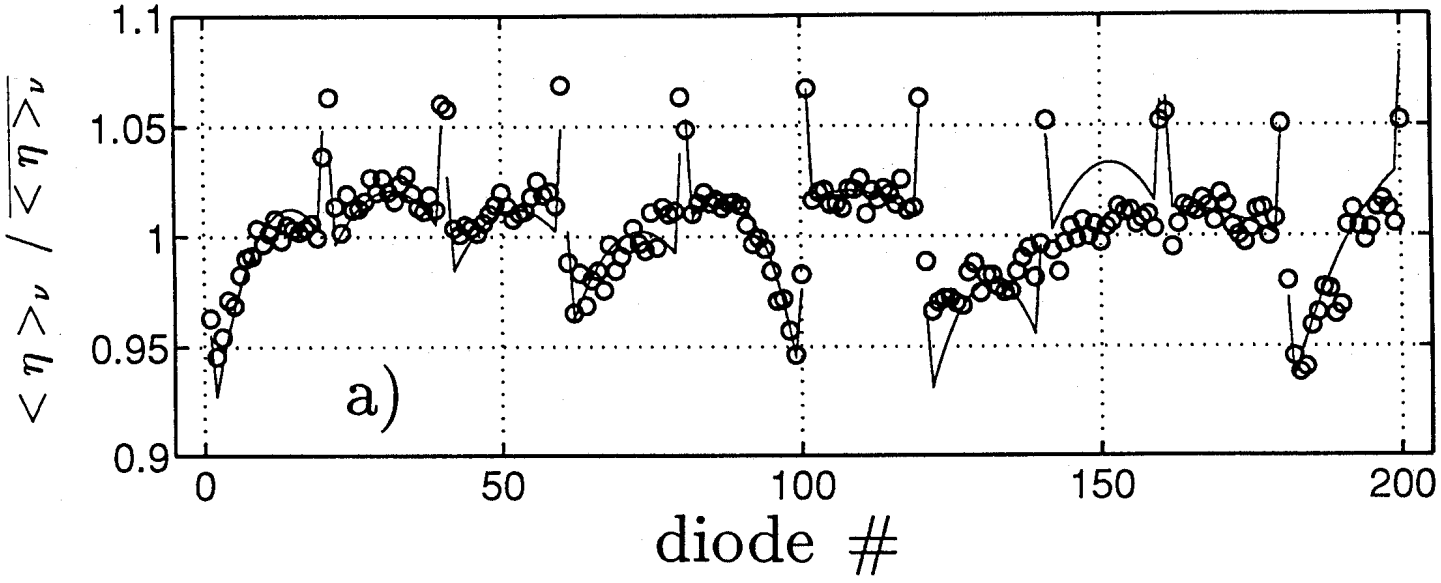
1.1
1.05
1
0.95
0.9
$<\eta>_\nu / \overline{<\eta>_\nu}$
a)
0
50
100
150
200
diode #

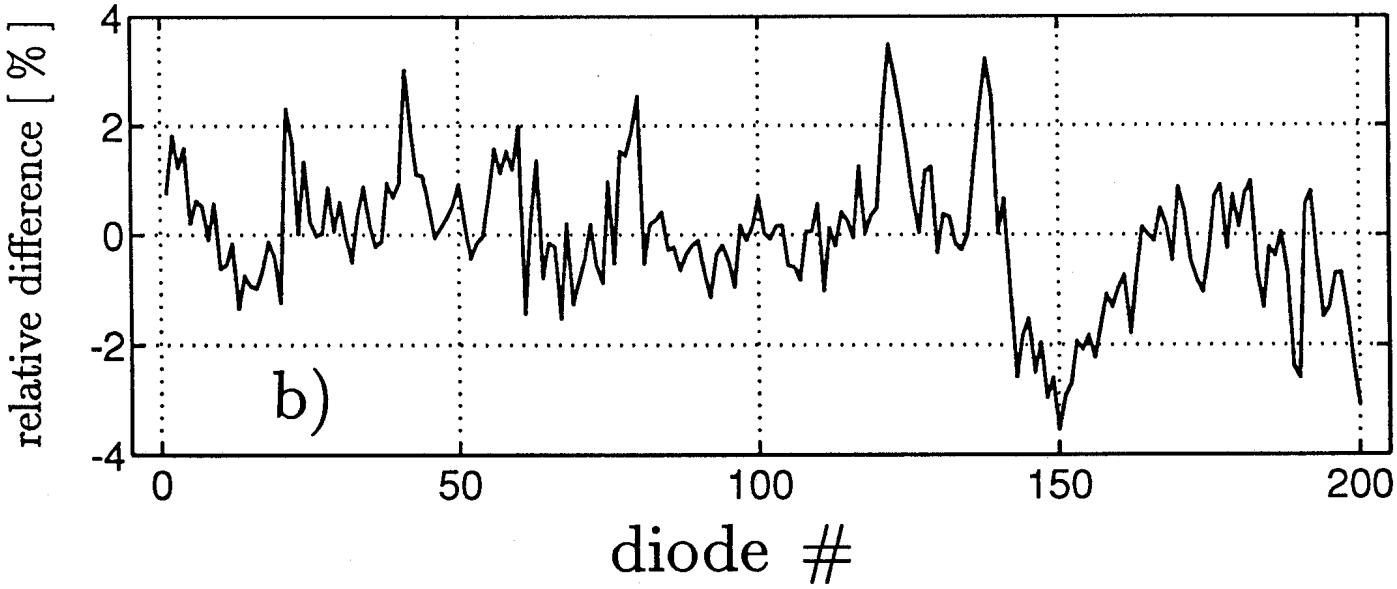
4
2
0
-2
-4
relative difference [%]
b)
0
50
100
150
200
diode #

fig. 12

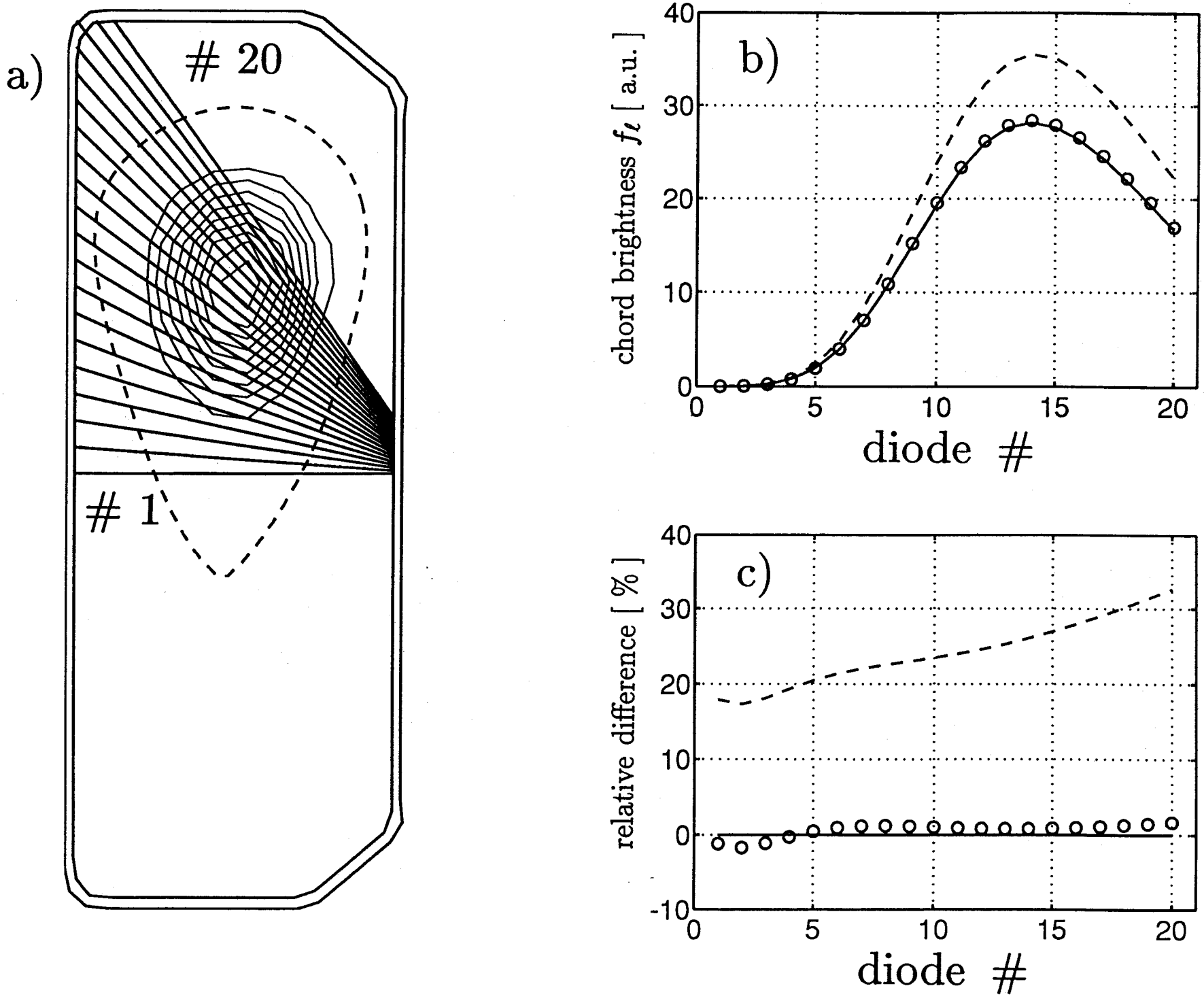
a)
20
1
b)
chord brightness f_l [a.u.]
diode #
c)
relative difference [%]
diode #

fig. 13

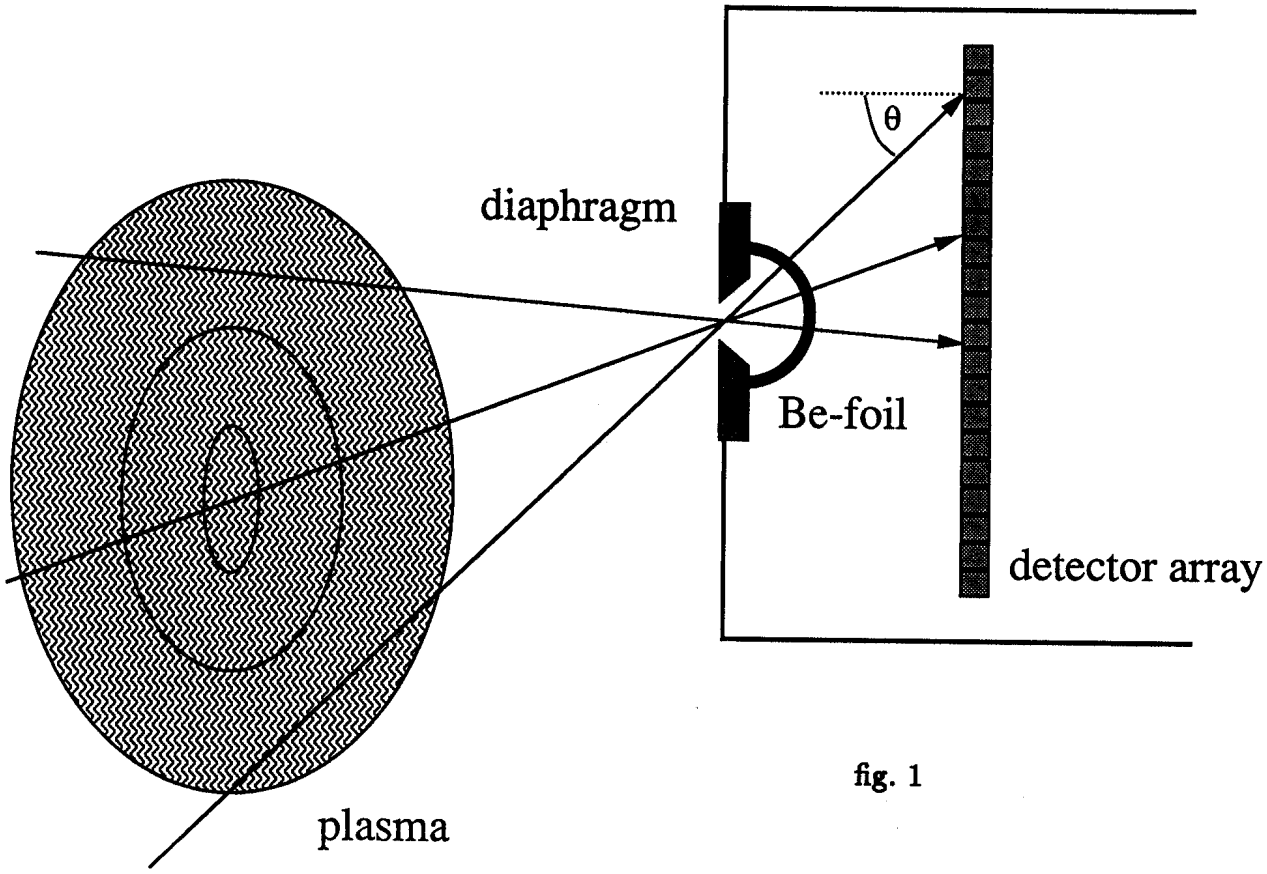
θ
diaphragm
Be-foil
detector array
plasma

fig. 1

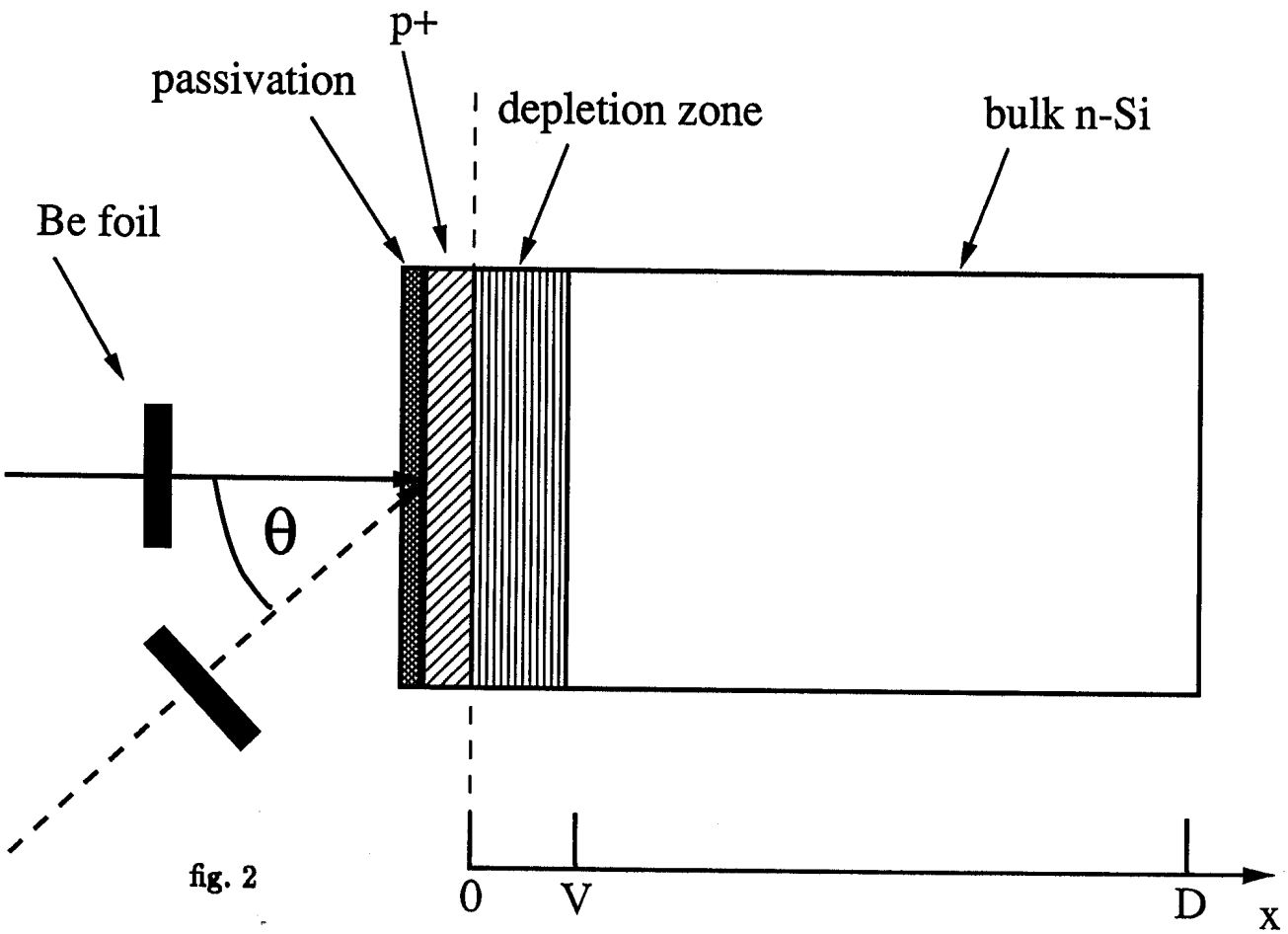
p+
passivation
depletion zone
bulk n-Si
Be foil
θ
0
V
D
x

fig. 2

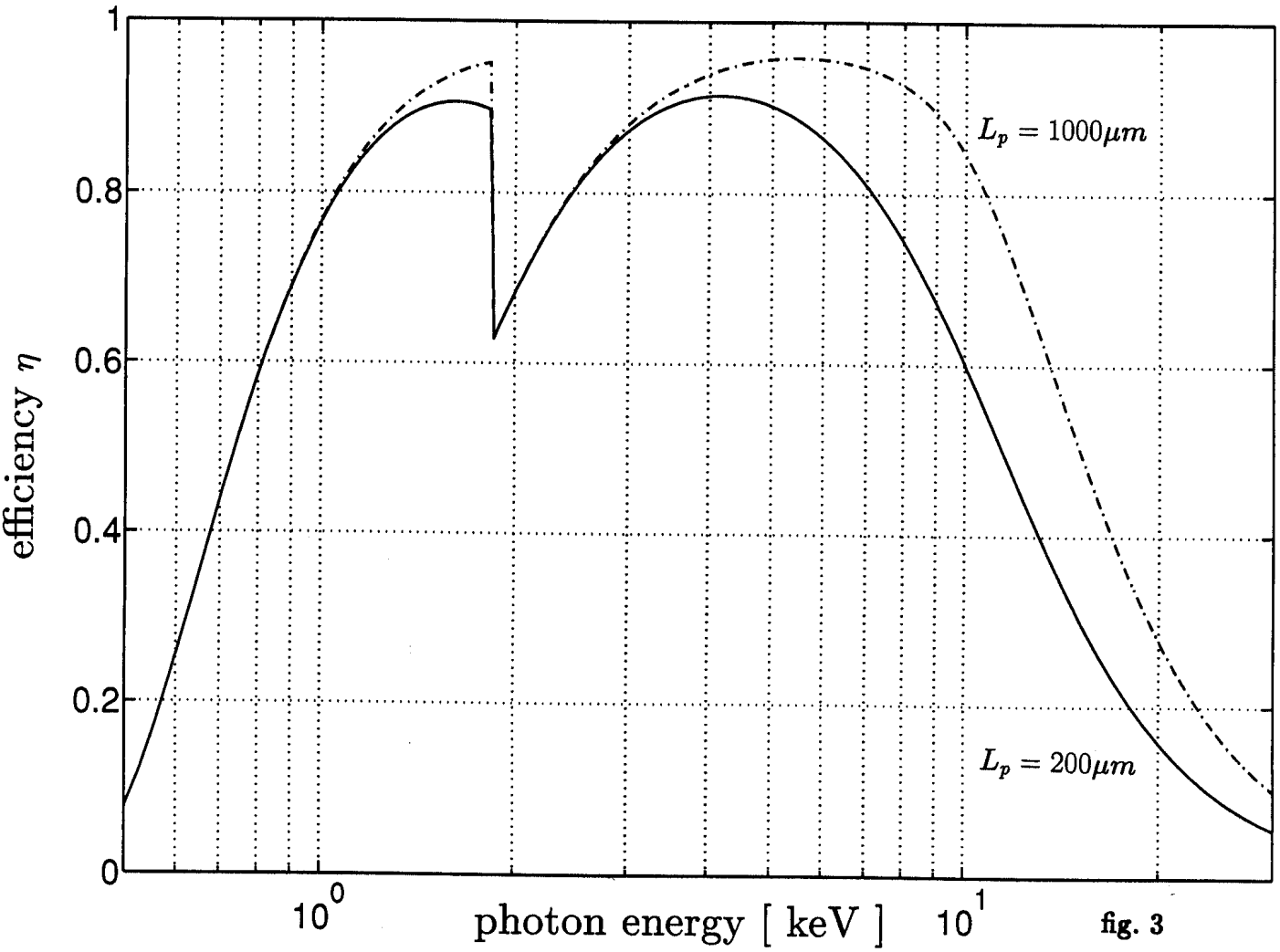
efficiency η
1
0.8
0.6
0.4
0.2
0
$L_p = 1000\mu m$
$L_p = 200\mu m$
10^0
10^1
photon energy [keV]

fig. 3

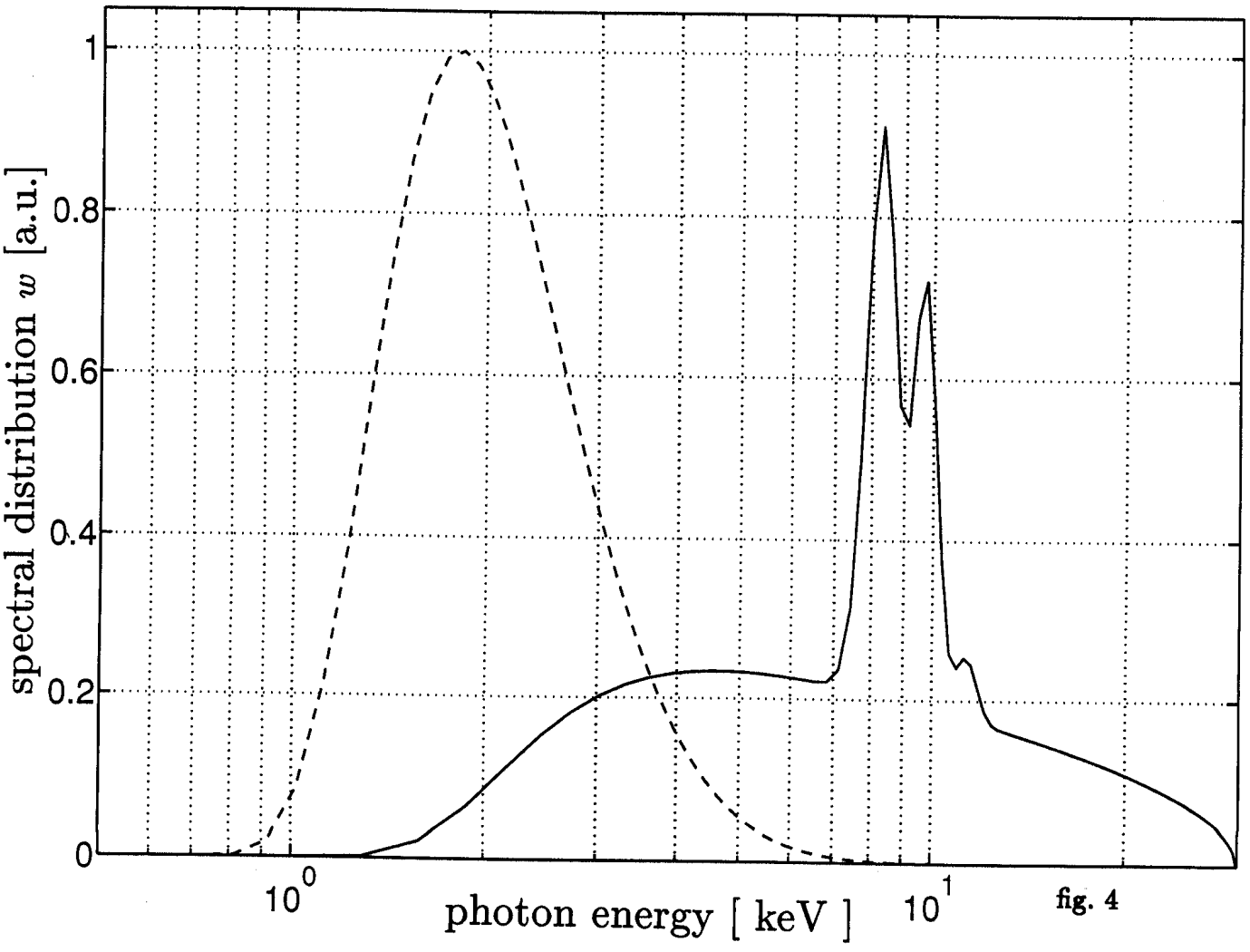
spectral distribution w [a.u.]
1
0.8
0.6
0.4
0.2
0
10^0
10^1
photon energy [keV]

fig. 4

fig. 5

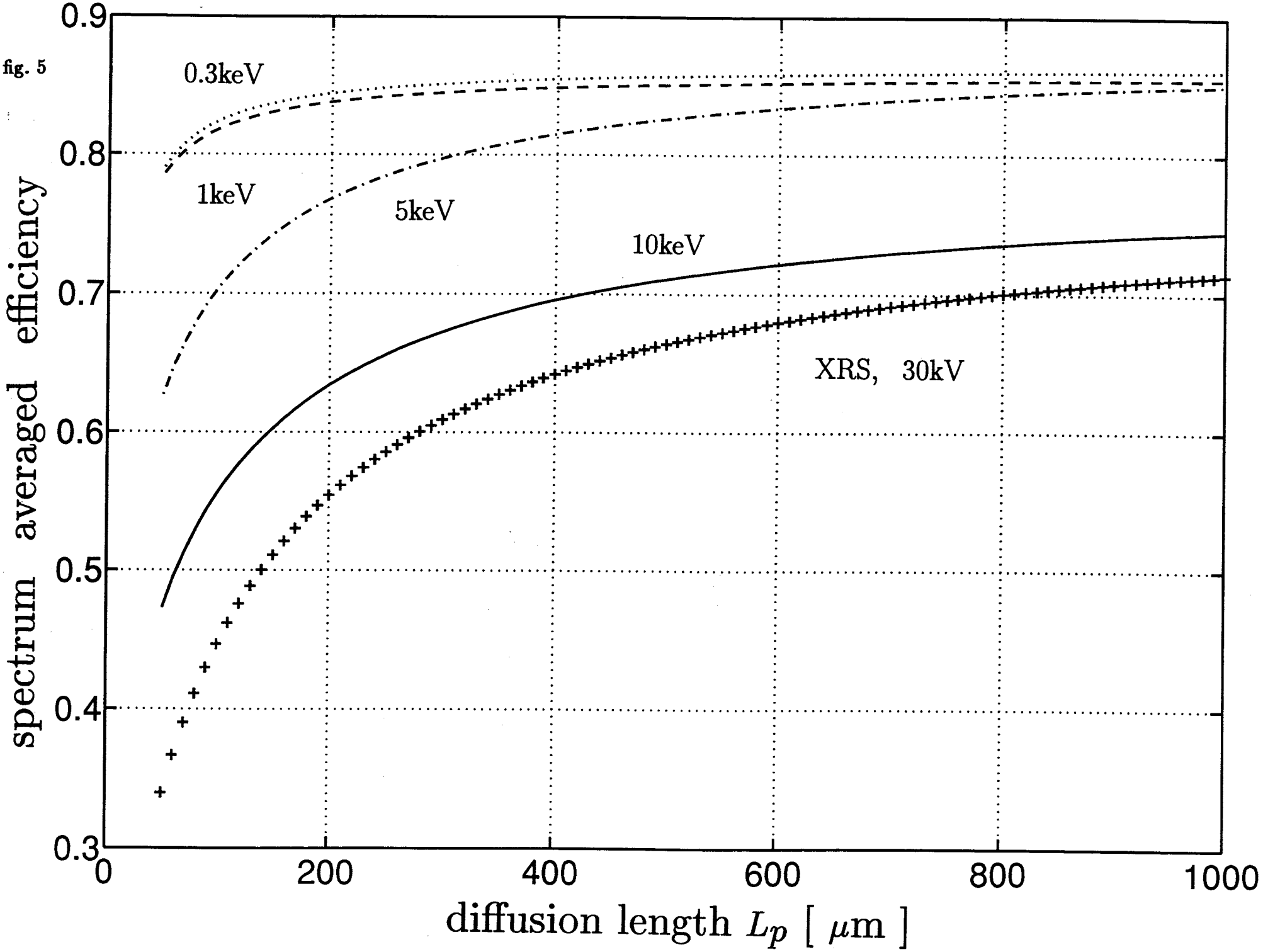
0.9
0.8
0.7
0.6
0.5
0.4
0.3
0
200
400
600
800
1000
spectrum averaged efficiency
diffusion length L_p [μm]
0.3keV
1keV
5keV
10keV
XRS, 30kV

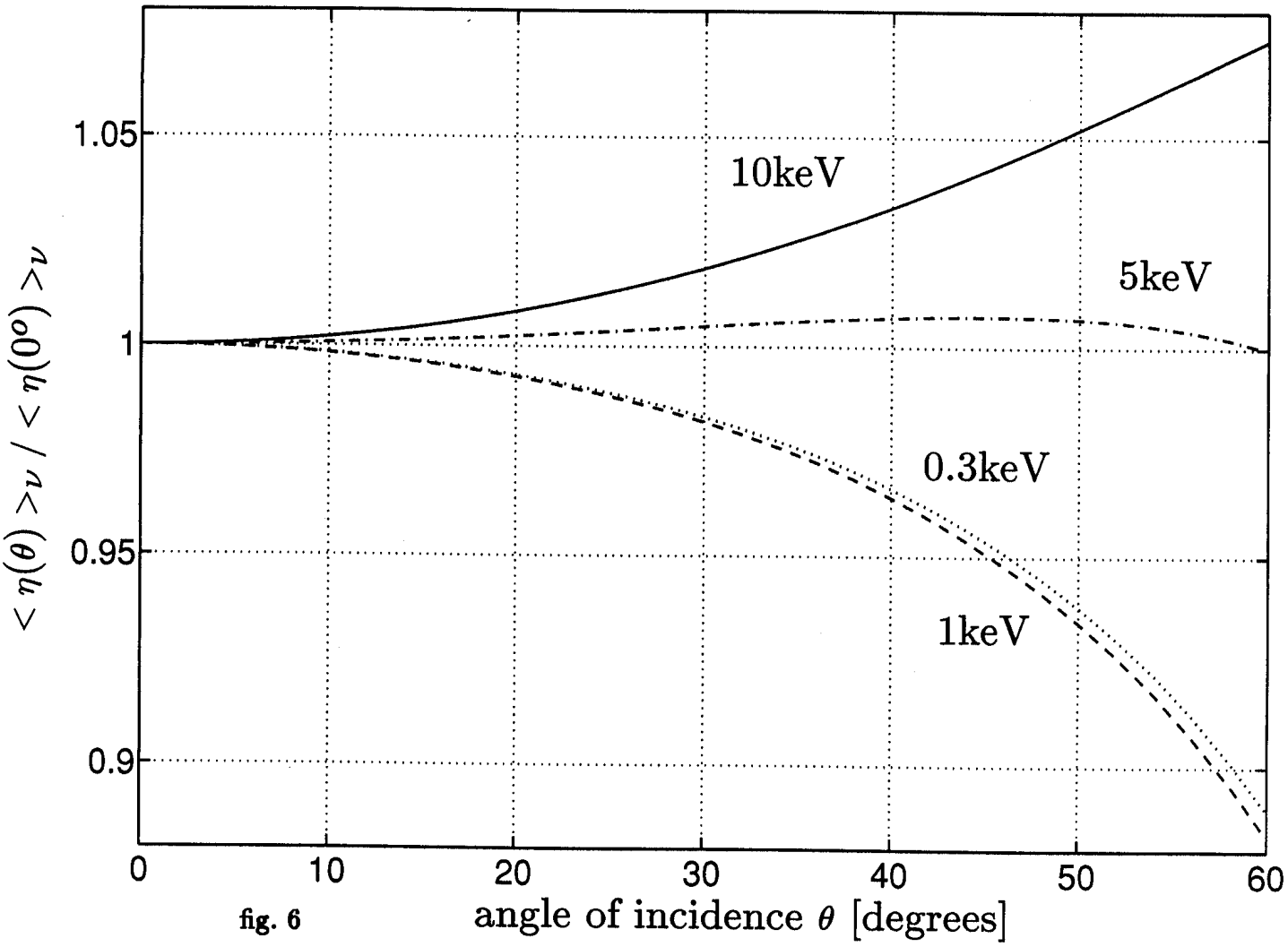
10keV
5keV
0.3keV
1keV
1.05
1
0.95
0.9
0
10
20
30
40
50
60
$< \eta(\theta) >_\nu / < \eta(0^o) >_\nu$
angle of incidence θ [degrees]

fig. 6

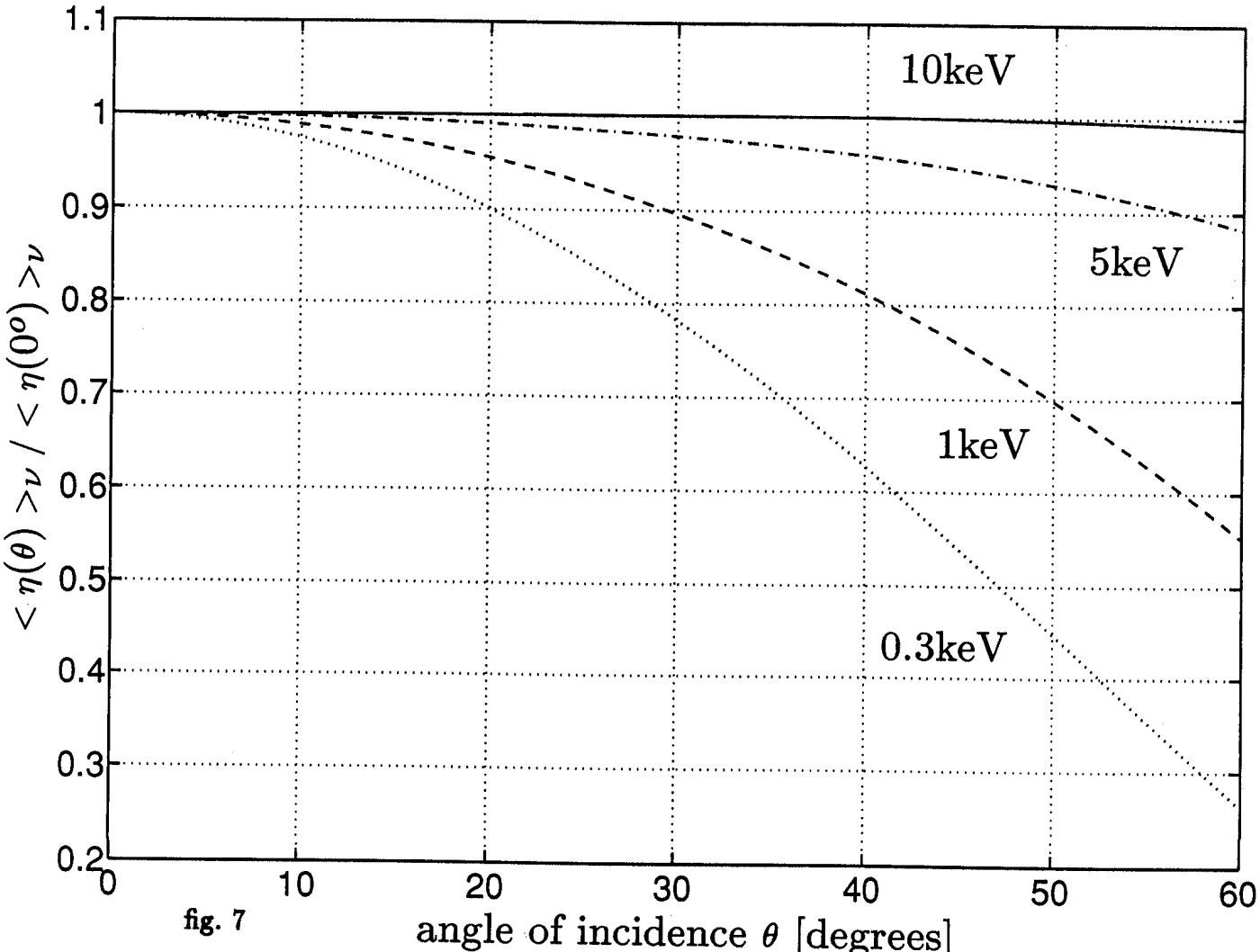
10keV
5keV
1keV
0.3keV
1.1
1
0.9
0.8
0.7
0.6
0.5
0.4
0.3
0.2
0
10
20
30
40
50
60
$< \eta(\theta) >_\nu / < \eta(0^o) >_\nu$
angle of incidence θ [degrees]

fig. 7

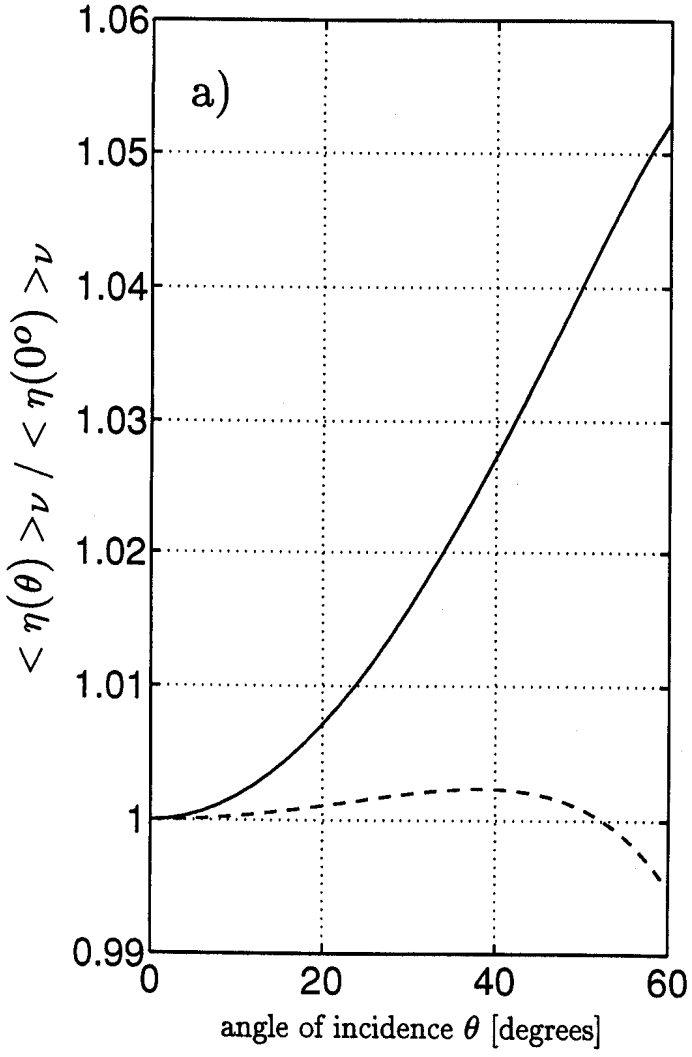
a)
1.06
1.05
1.04
1.03
1.02
1.01
1
0.99
0
20
40
60
$< \eta(\theta) >_\nu / < \eta(0^o) >_\nu$
angle of incidence θ [degrees]

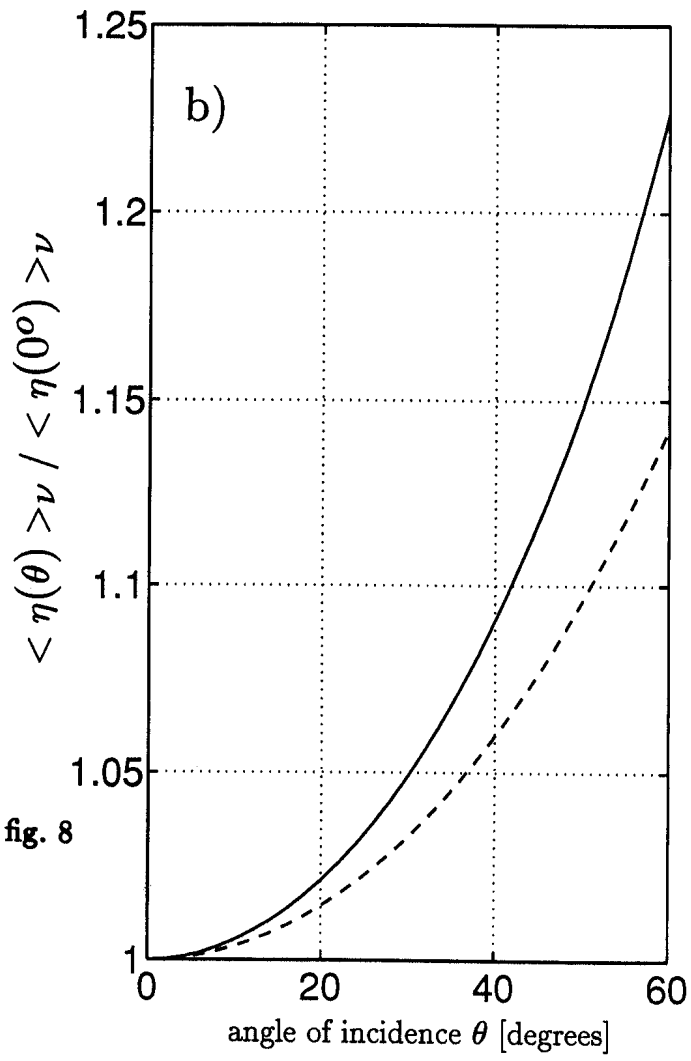
b)
1.25
1.2
1.15
1.1
1.05
1
0
20
40
60
$< \eta(\theta) >_\nu / < \eta(0^o) >_\nu$
angle of incidence θ [degrees]

fig. 8

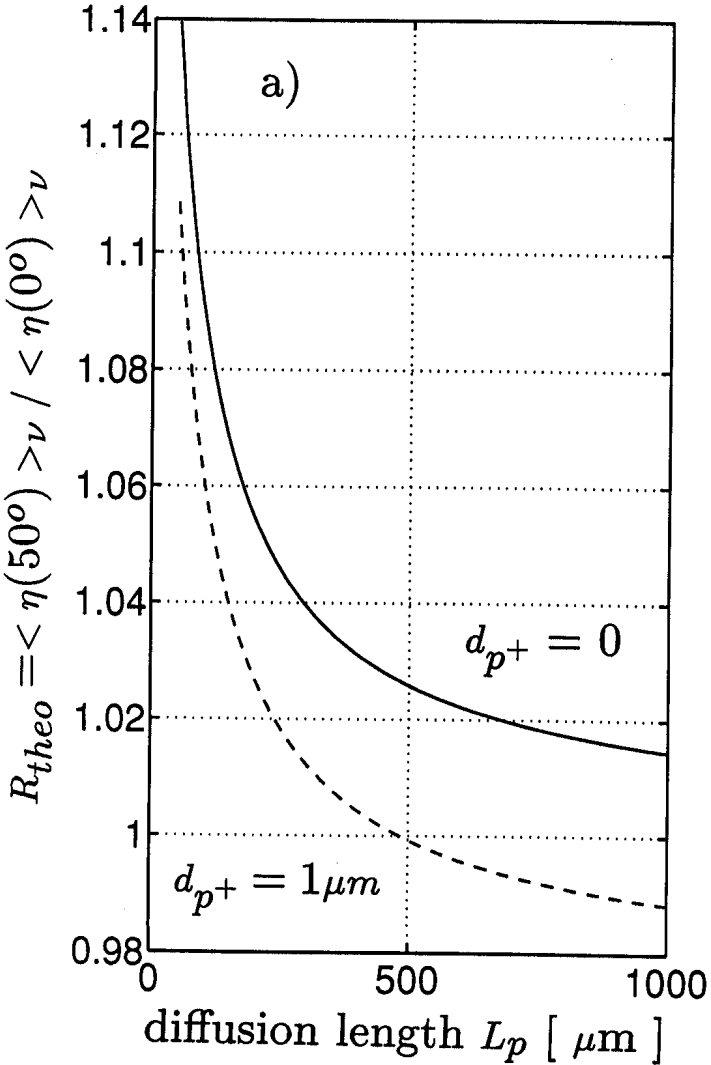
a)
1.14
1.12
1.1
1.08
1.06
1.04
1.02
1
0.98
0
500
1000
$R_{theo} = < \eta(50^o) >_\nu / < \eta(0^o) >_\nu$
$d_{p^+} = 0$
$d_{p^+} = 1\mu m$
diffusion length L_p [μm]

fig. 9

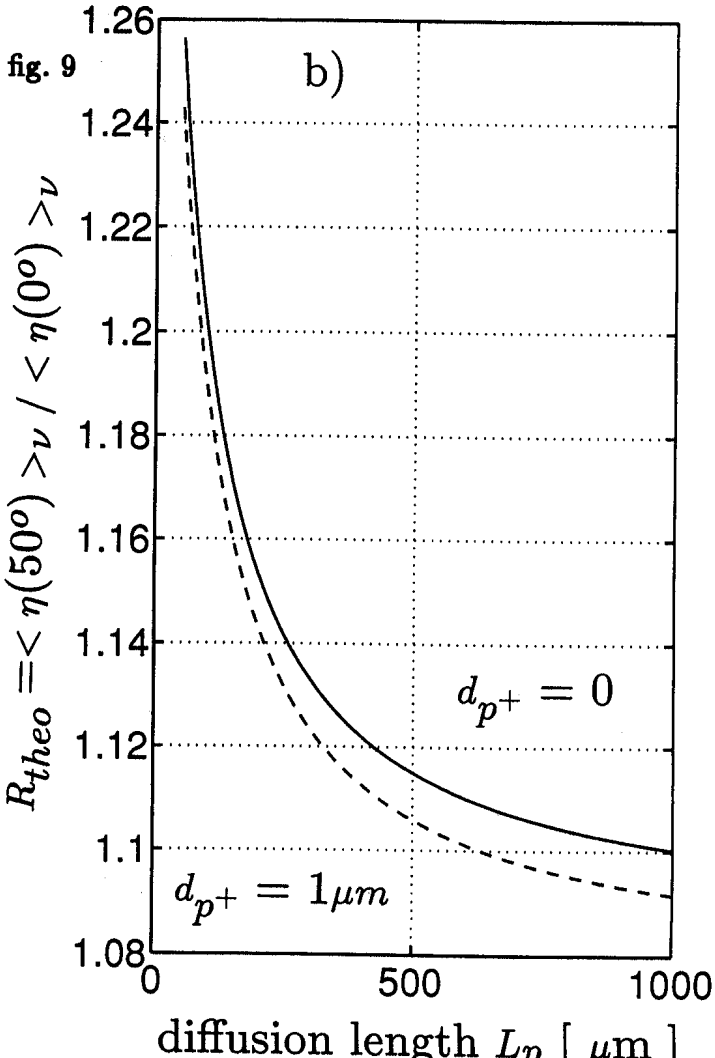
b)
1.26
1.24
1.22
1.2
1.18
1.16
1.14
1.12
1.1
1.08
0
500
1000
$R_{theo} = < \eta(50^o) >_\nu / < \eta(0^o) >_\nu$
$d_{p^+} = 0$
$d_{p^+} = 1\mu m$
diffusion length L_p [μm]

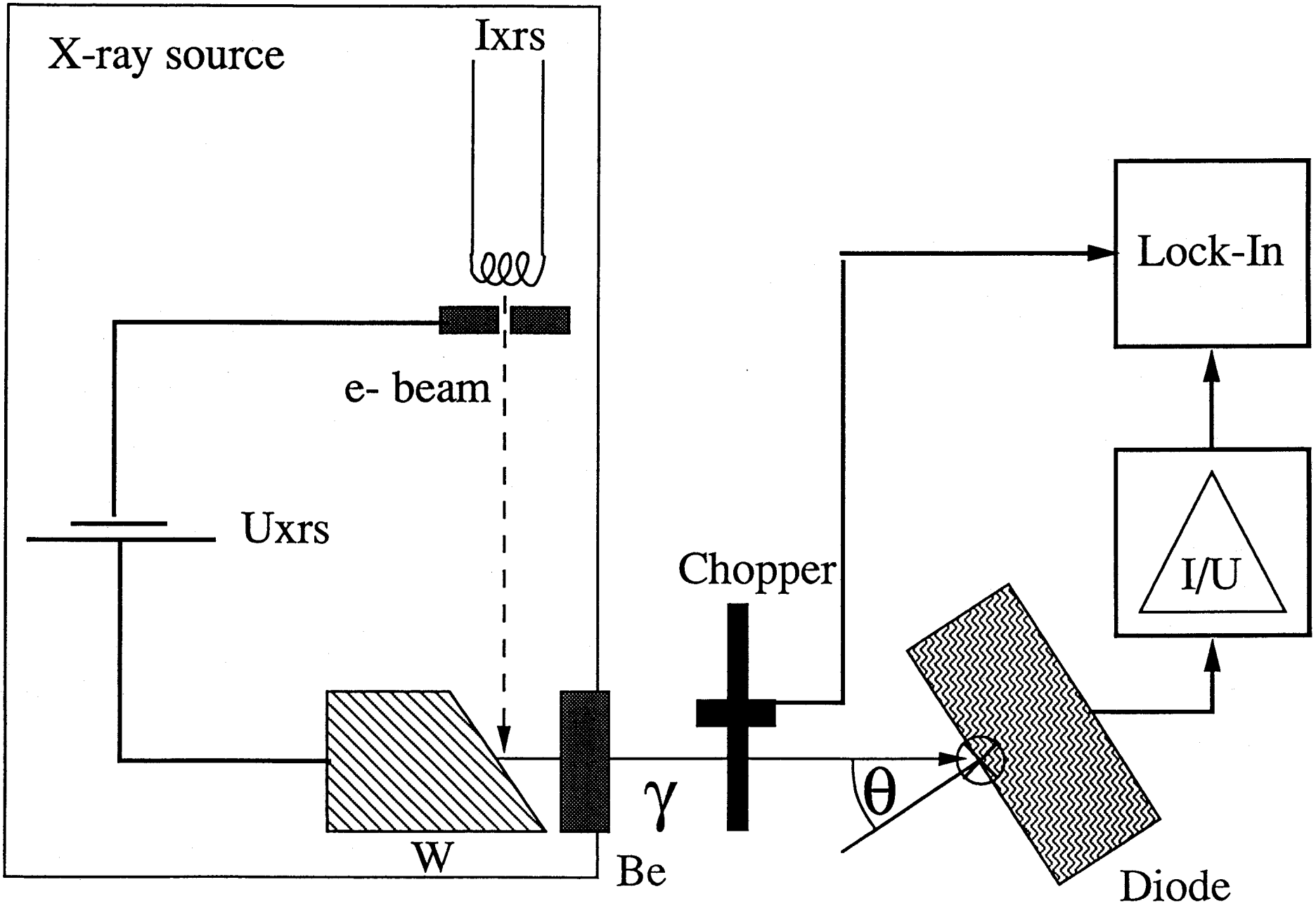

fig. 10

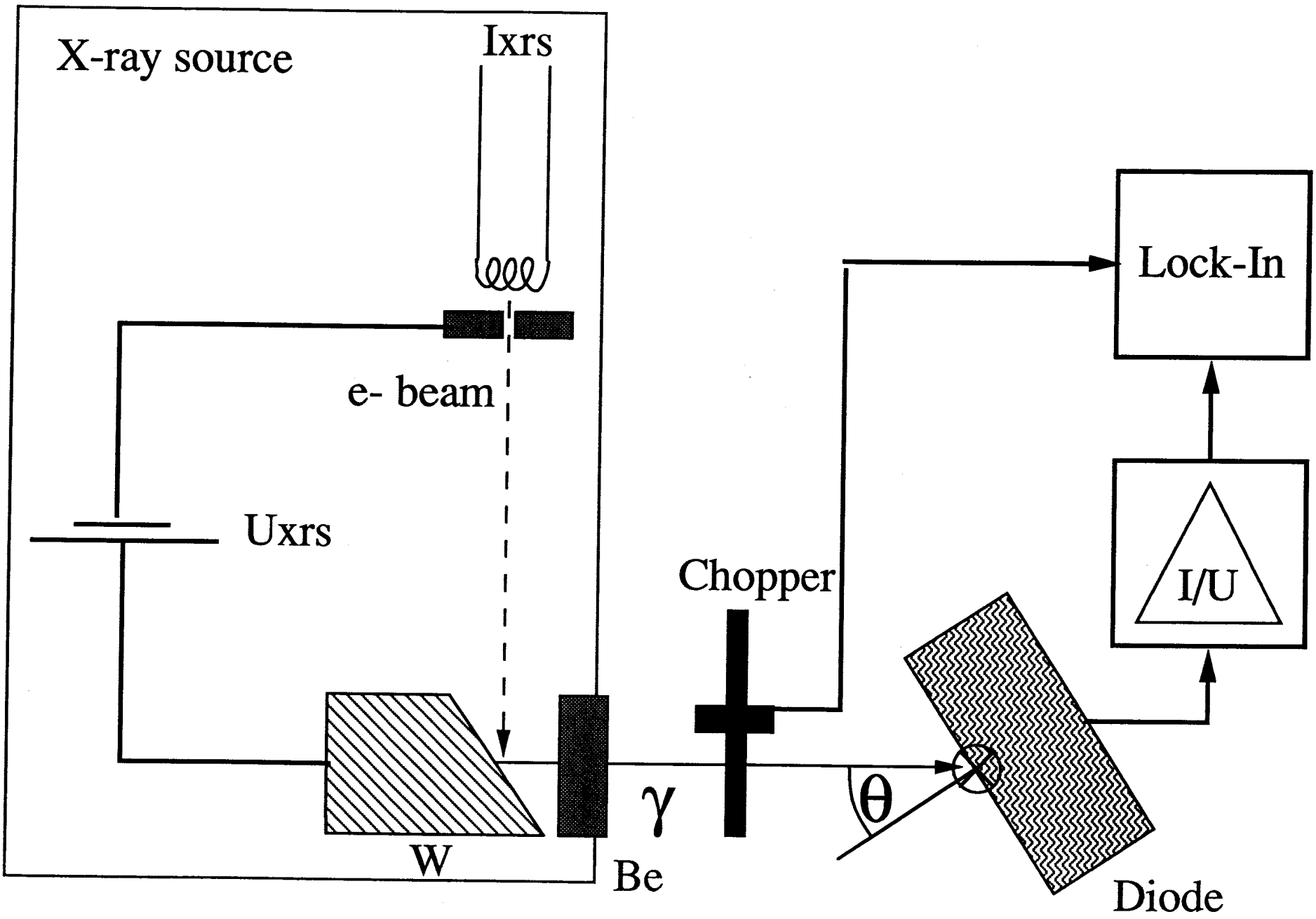

fig. 10

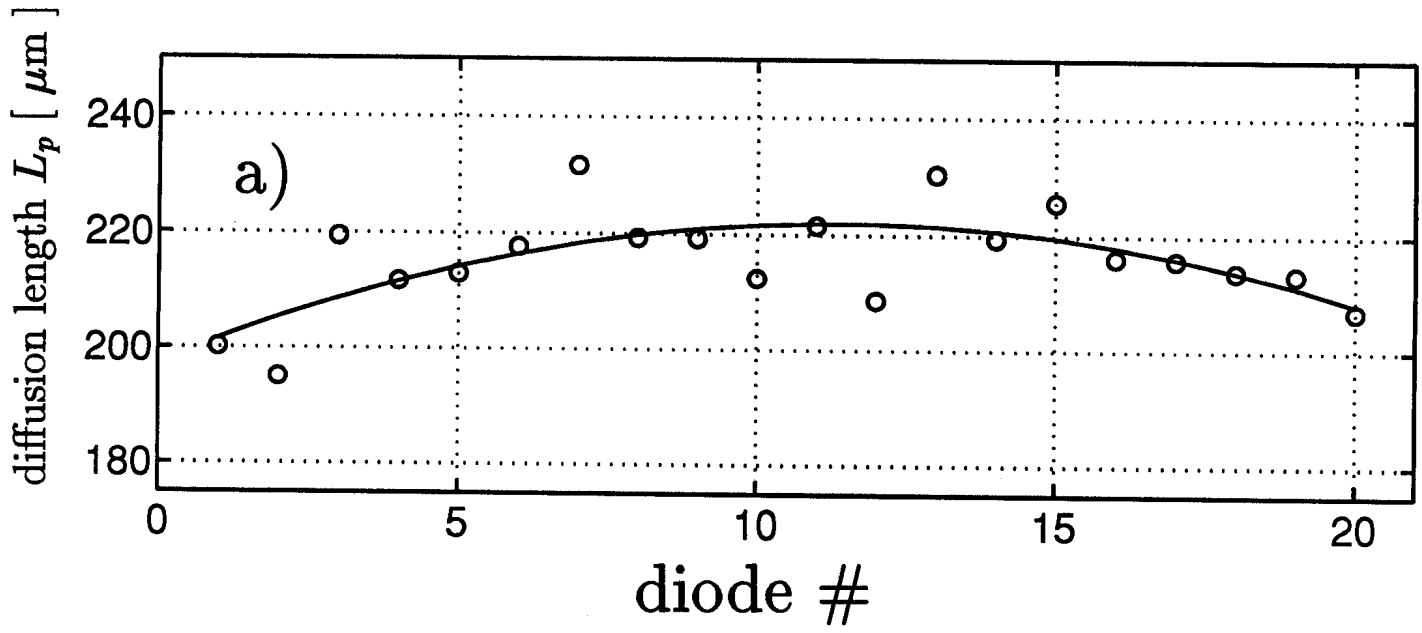
diffusion length L_p [μm]
240
220
200
180
a)
0
5
10
15
20
diode #

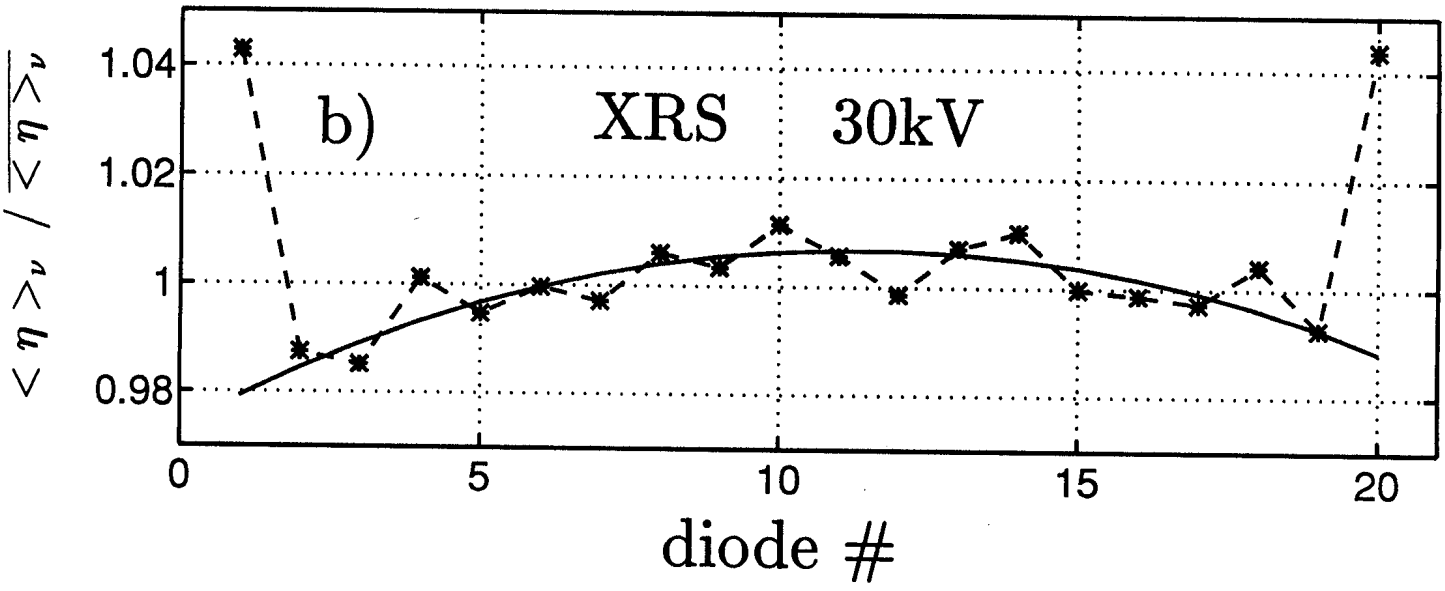
$< \eta >_\nu \; / \; \overline{< \eta >_\nu}$
1.04
1.02
1
0.98
b)
XRS
30kV
0
5
10
15
20
diode #

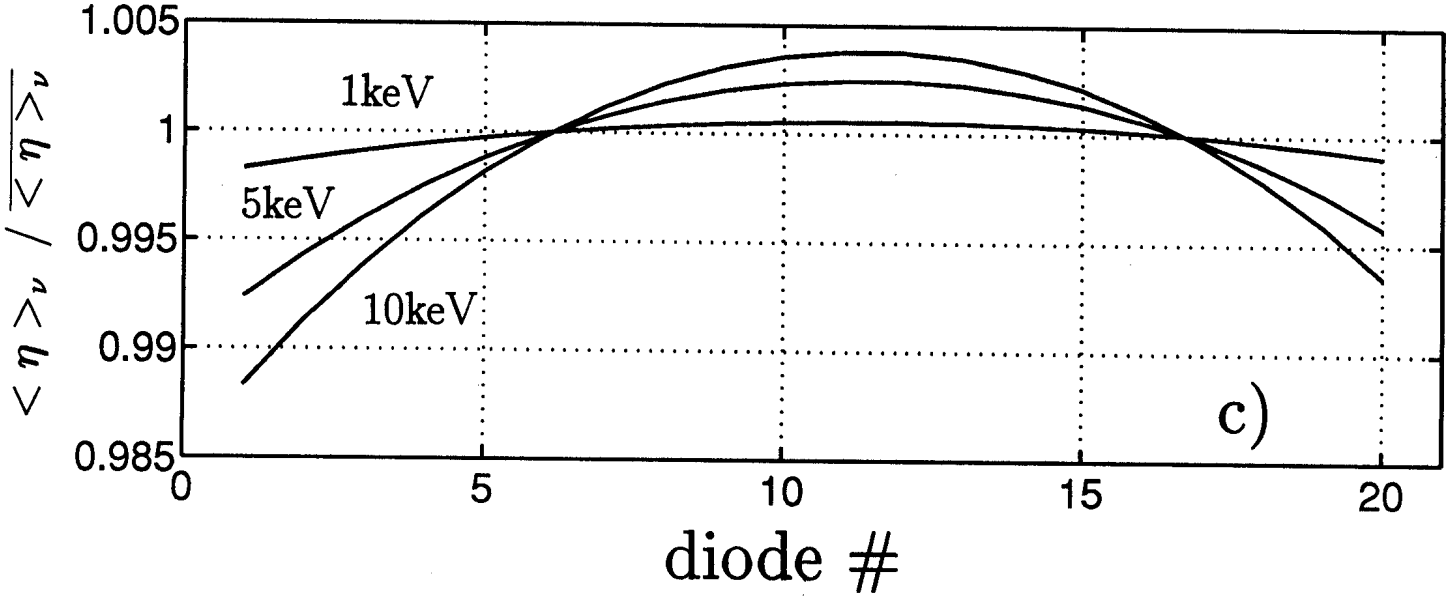
$< \eta >_\nu \; / \; \overline{< \eta >_\nu}$
1.005
1
0.995
0.99
0.985
1keV
5keV
10keV
c)
0
5
10
15
20
diode #

fig. 11

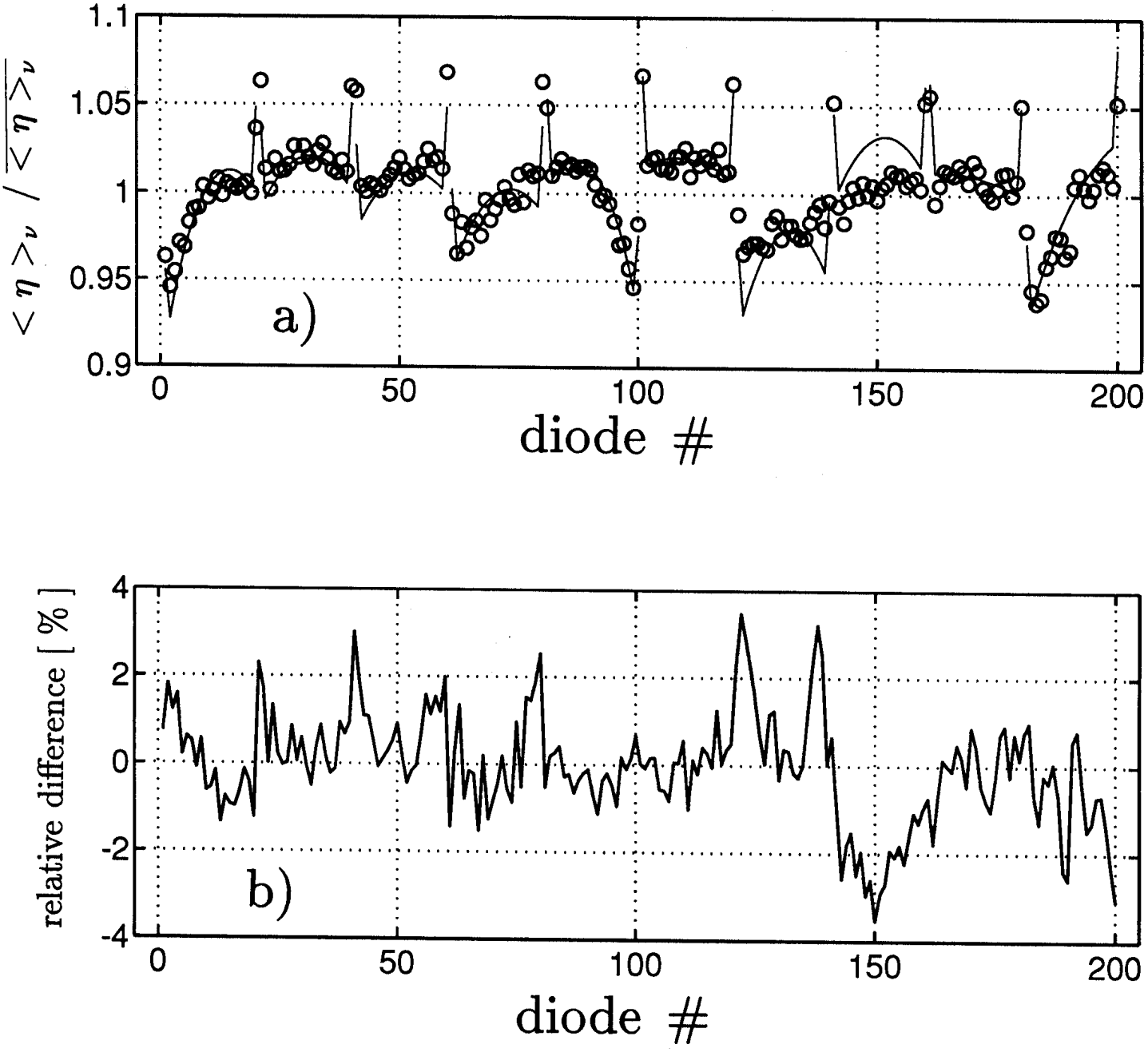
1.1
1.05
1
0.95
0.9
$< \eta >_\nu \; / \; \overline{< \eta >_\nu}$
a)
0
50
100
150
200
diode #

4
2
0
-2
-4
relative difference [%]
b)
0
50
100
150
200
diode #

fig. 12

a)
20
1
b)
chord brightness f_i [a.u.]
diode #
c)
relative difference [%]
diode #

fig. 13